OPTIMISATION OF MOTION AND FORCE TRANSMISSIONS IN A SINGLE-TOGGLE JAW CRUSHING MECHANISM

JOSEPH KIMANI MWANGI

MASTER OF SCIENCE
(Mechanical Engineering)

JOMO KENYATTA UNIVERSITY OF AGRICULTURE AND TECHNOLOGY

2022

Optimisation of Motion and Force Transmissions in a Single-Toggle Jaw Crushing Mechanism

Joseph Kimani Mwangi

A Thesis Submitted in Partial Fulfilment of the Requirements for the Degree of Master of Science in Mechanical Engineering of the Jomo Kenyatta University of Agriculture and Technology

2022

DECLARATION

This thesis is my original work and has not been presented for a degree in any other university.

Signature..... Date...../...../.....

Joseph Kimani Mwangi

This thesis has been submitted for examination with our approval as university supervisors:

Signature..... Date...../...../.....

Dr. Onesmus Mutuku Muvengei, PhD

JKUAT, Kenya

Signature..... Date...../...../.....

Eng. Prof. John M. Kihiu

JKUAT, Kenya

DEDICATION

This work is dedicated to my lovely parents, Mr. Julius Mwangi Macharia and Mrs. Irine Wangeci Mwangi for their unwavering support and prayers throughout my studies. I also dedicate it to the late Prof. Moses F. Oduori who was my supervisor until he passed on in 2018.

ACKNOWLEDGMENT

My greatest gratitude goes to the Almighty God for His divine guidance and protection throughout my study. I appreciate my supervisors, Dr. Onesmus M. Muvengei and Eng. Prof. John M. Kihiu for their priceless guidance and counsel all the way. I am also grateful to Dr. James K. Kuria and Dr. Jackson G. Njiri for their support and motivation during my study period. I am as well grateful to my friends Peter Mwangi, Justin Byiringiro and Philbert Muhayimana with whom we have journeyed together. My deep gratitude to the Jomo Kenyatta University of Agriculture and Technology (JKUAT) for granting me a scholarship to pursue this study. Finally, I thank colleagues and members of the SOMMME Postgraduate seminar for their thoughtful input to this research.

TABLE OF CONTENTS

LIST OF TABLES

LIST OF FIGURES

LIST OF APPENDICES

LIST OF ABBREVIATIONS

AutoCAD	Autodesk Computer Aided Design
DE	Differential Evolution
DEPSO	Differential Evolution Particle Swarm Optimisation
DOFs	Degrees of Freedom
EA	Evolutionary Algorithms
EFR	Effective Force Ratio
FTI	Force Transmission Index
GA	Genetic Algorithm
IPSO	Improved Particle Swarm Optimisation
JFI	Joint Force Index
JMM	Jacobian Matrix Method
MA	Mechanical Advantage
MATLAB	Matrix Laboratory
MSC	MacNeal-Schwendler Corporation
ADAMS	Automated Dynamic Analysis of Mechanical Systems
MSMEs	Micro, Small and Medium Enterprises
PSO	Particle Swarm Optimisation
SGR	Standard Gauge Railway

LIST OF SYMBOLS

α	Nip angle [degrees]
α_{ij}	Angle between f_{ji} and v_{ij} [degrees]
a_{opt}	Optimum crank length [mm]
a_{range}	Range of crank lengths [mm]
A_X	Area under shearing travel graph [mm]
A_Y	Area under crushing travel graph [mm]
β	Inclination angle of the swing jaw [degrees]
b_{opt}	Optimum coupler length [mm]
b_{range}	Range of coupler lengths [mm]
c_{opt}	Optimum rocker length [mm]
c_{range}	Range of rocker lengths [mm]
d_{opt}	Optimum frame length [mm]
d_{range}	Range of frame lengths [mm]
F	Weight of rocks in crushing chamber [N]
g	Gravitational acceleration [m/s^2]
γ	Angular position of toggle plate [degrees]
H	Range of horizontal motion [mm]
L_0	Length of the frame [mm]
L_1	Eccentricity of the eccentric shaft [mm]
L_2	Length of the swing jaw [mm]
L_3	Length of the toggle plate [mm]
m	Mass of swing jaw [kg]
μ	Material loosening coefficient
n	Rotation speed of the eccentric shaft [rpm]
ν	Velocity of the swing jaw [m/s]

P_C	Compressive load on the swing jaw [N]
P_S	Shearing load on the swing jaw [N]
φ	Inclination of the toggle plate [degrees]
Q	Capacity of jaw crusher [m^3/s]
R	Crushing ratio, B/b,
r_1	Length of fixed link [mm]
r_2	Length of crank [mm]
r_3	Length of coupler [mm]
r_4	Length of rocker [mm]
ρ	Density of the feed material [kg/mm^3]
S_{av}	Average compression stroke of the moving jaw [mm]
t	Time interval [s]
θ	Crank angle [degrees]
T_{in}	Input torque [Nmm]
T_{out}	Loading moment of unity intensity [Nmm]
V	Range of vertical motion [mm]

ABSTRACT

Jaw crushers are important mechanisms in quarries and construction sites used to reduce rocks and stones into aggregate materials for construction works. These crushers are also used in the mining industry to prepare the ore for secondary milling processing by reducing it to suitable sizes. The single-toggle jaw crusher is the most common crusher and uses a swing jaw which crushes the feed material against a fixed jaw. The crushing process is achieved through the application of both motion and force. The swing jaw moves back and forth towards the fixed jaw while transmitting forces from a motor-coupled eccentric shaft. For the feed material to be crushed, the mechanism must supply enough compressive force to overcome the compressive strength of the feed. This research was concerned with the synthesize of jaw crusher mechanisms which achieves optimal force and motion transmission from the input eccentric shaft to the ouput swing jaw. The aim was to ensure maximum crushing motion for better rock comminution as well as minimising shearing motion for wear reduction. In addition, the research investigated optimal force application on the rocks to overcome their fracture toughness and reduction to small particle sizes. The research involved the use of evolutionary optimisation technique called Genetic Algorithm (GA) to search for optimum link sizes that gave the best transmission results. Genetic Agorithm was implemented using MATLAB software. Motion optimisation was divided into two sections namely, crushing-shearing ratio and crush-travel inverse. Force optimisation was also split into two: static force and dynamic force and an objective function for each was created and fed into the GA solver. All objective functions were developed from first principles and then coded in MATLAB. Four optimised designs were synthesised each corresponding to the crusher motion or force parameter being optimised. The motion crushing-shearing ratio optimised design had 1.18 times higher crushing than shearing. The crushing-only optimised design achieved a production rate of 1.7 $\times 10^{-4}$ m^3. Meanwhile, the static force optimised design gave a total torque of 425 MNm while the dynamic force optimised design resulted in a total dynamic torque of 640GNm. The effect of link lengths on the four criteria were also sought and established. The swing jaw had the highest influence on both motion and force transmission so that a longer swing jaw was preferrable. The findings from this study will assist in the production of a new, optimised and locally fabricated single-toggle jaw crusher with high crushing efficiency, power saving and increased production. These findings will also aid in the modification of the existing ones by varying lengths of the components to increase crusher production via optimised motion and force transmission.

CHAPTER ONE

INTRODUCTION

1.1 Background

Infrastructure development worldwide, whether roads, bridges, or buildings rely heavily on the use of stones. Stones are obtained from rocks which are the main components of the earth's crust thus explaining their common usage in construction. The global demand for construction aggregate was poised to rise by 2.3% to reach 47.5 billion metric tons by 2023 with the demand for crushed stones being twice that of sand and gravel (Freedonia, 2019). In Kenya, demand for aggregates has risen steadily since 2003 when the government stepped up investment on road projects Bloomberg (2019). The most recent infrastructure project was the Standard Gauge Railway (SGR); Phase 2A of the project used more than $600,000$ metric tonnes of manufactured sand, which was composed of crushed rocks and quarry stones as a substitute for sand and gravel (Langat, 2019; Muiruri, 2019). Manufactured sand has gained popularity since the sand and gravel resources are becoming depleted (Thuita, 2017). Therefore, contractors are opting to use crushed rocks in concrete for riverine ecosystems conservation as well as cheaper production.

Rock or stone crushing can be divided into large-scale and small-scale categories. Large-scale stone crushing utilizes crushing machines, which are usually imported, to comminute several tonnes of stones into desired sizes. Despite the effectiveness of these machines in comminution, the initial and operating costs involved are high. These limitations are responsible for the scarce availability of such machines around the country with most construction companies opting for small-scale rock crushing (Munyasi & Oduori, 2012). In this second category, stones are crushed by several

people each using a hammer and an anvil in a process that is highly dependent on human energy. The manual nature of small-scale crushing makes it less productive, less profitable, and hazardous (Munyasi & Oduori, 2012). In this regard, there is need to provide the small-scale construction enterprises with affordable, safer, more productive, and more profitable method of stone crushing.

Jaw crushers are the commonest means of primary rock crushing where the production rate is below 1,000 metric tonnes per hour (Donovan, 2003). The general operation of a jaw crusher involves a moving swing jaw crushing the rock feed against a stationary fixed jaw. There are three types of jaw crushers used in the mining and quarrying industry namely: The Blake crusher, dodge crusher and the universal crusher as shown in Figure 1.1. The categorization is dependent on the location of the pivot for the swing jaw (Wills & Napier-Munn, 2006).

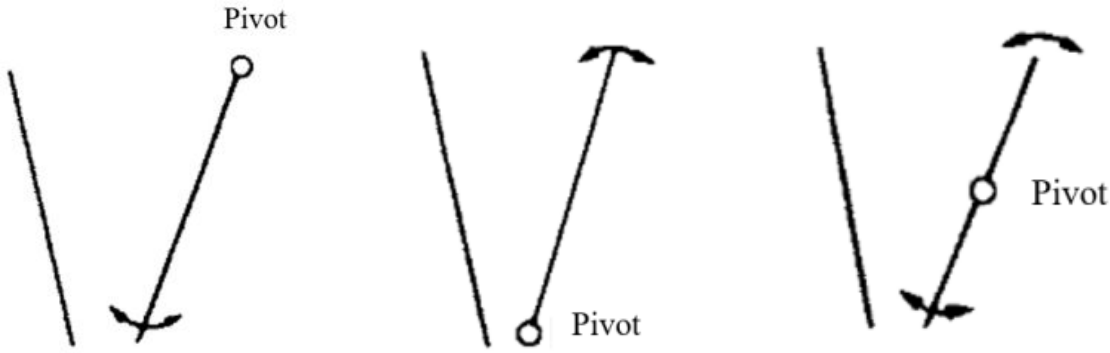

(a) Blake Crusher (b) Dodge Crusher (c) Universal Crusher

Figure 1.1: Types of Jaw Crushers (Wills & Napier-Munn, 2006)

The Blake crusher is the most popular type in use today and it has two variants, the single-toggle jaw crusher and the double toggle jaw crusher which are shown in Figure 1.2 (Suresh, 2009).

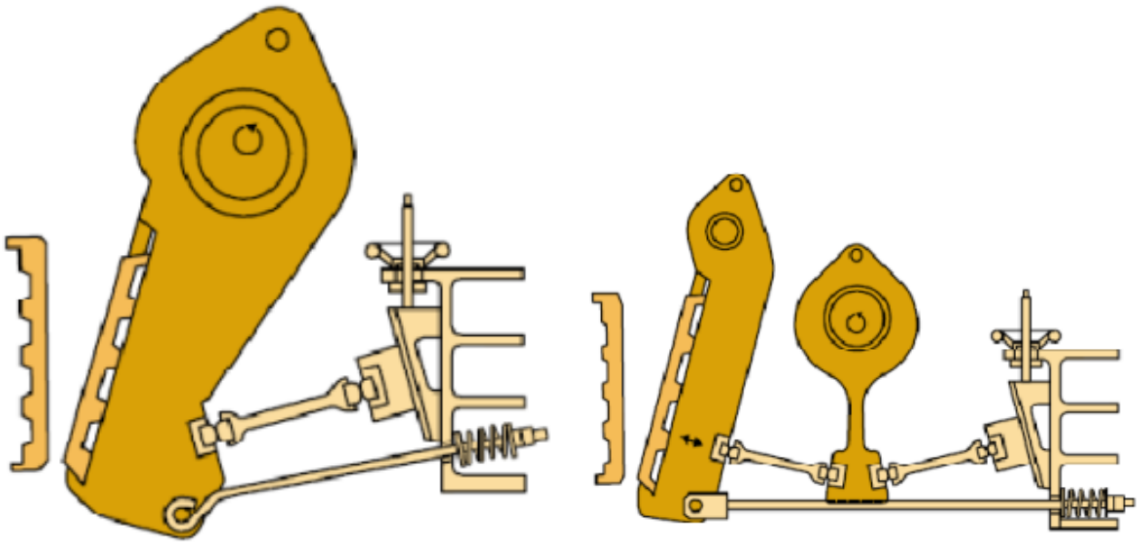

(a) Single-toggle jaw crusher (b) Double toggle jaw crusher

Figure 1.2: Variants of the Blake jaw crusher (Suresh, 2009)

A double-toggle Blake crusher is larger and heavier compared to the single-toggle Blake crusher. In addition, the swing jaw of the double-toggle design only moves horizontally towards the fixed jaw. Meanwhile, the swing jaw of the single-toggle design has elliptical motion providing for the much needed throughput via its vertical motion. Consequently, a single-toggle crusher has greater capacity compared to a double-toggle crusher of the same size. Furthermore, a double-toggle crusher costs about 50% more than a similarly sized single-toggle machine. The single-toggle jaw crusher is, therefore, the most preferred design suitable for rock crushing in Micro, Small and Medium enterprises (MSMEs). The single-toggle jaw crusher is popular in quarrying and building operations since its simplified and lighter construction makes it easily portable. Other benefits of the single-toggle jaw crusher include the ease of adjustment to suit the materials being crushed and its simplified maintenance procedures (McNally, 2003). However, despite the numerous advantages of the single-toggle crusher, the vertical motion of the swing jaw is responsible for the rapid wear of the crushing surfaces.

A preliminary design of the single-toggle jaw crusher was as shown Figure 1.3. More research was suggested to optimise the design so as to make it more affordable, more accessible and more productive to the small-scale stone crushing businesses in comparison with the crushers available in the market (SCM, 2020).

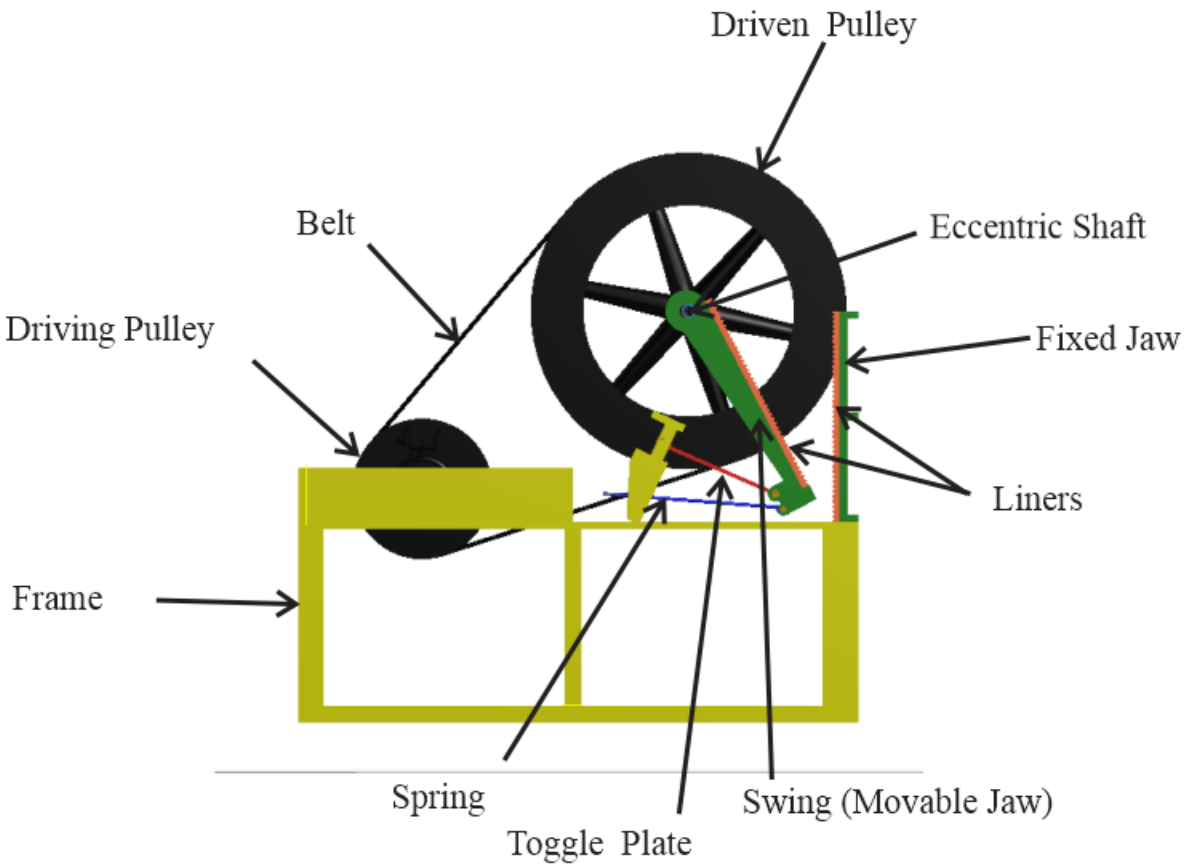

Figure 1.3: Preliminary Design of the Proposed Single-Toggle Jaw Crusher

The working principle of the mechanism involves crushing the feed material fed at the top in between the fixed jaw and the moving jaw. The moving jaw is powered by the motor or engined-coupled eccentric shaft and its movement is controlled by the toggle plate and the spring. The crushed particles are nipped and gradually reduce in size until they drop out at the bottom of the jaws once their sizes reduce below that of the closed set. The closed set is the case when the swing jaw is nearest to

the fixed jaw.

It is important to understand the crushing process in a single-toggle jaw crusher. These are compressive machines with the eccentric shaft as the power source and controlled by the toggle plate to produce high crushing forces. When feed material gets into the crushing chamber, the swing jaw moving towards the fixed jaw applies compressive force on the rocks and causes them to fail.

The feed material fails in two ways: abrasion and cleavage fracture. Abrasion failure occurs at the areas in direct contact with the jaws due to localised compressive stresses as shown at the top and bottom parts of Figure 1.4a (Donovan, 2003). However, cleavage fracture is the main form of failure and occurs inside the rock material as a result of induced tensile stresses. This is because rocks are about ten times weaker in tension than in compression. The induced tensile forces lead to the formation of a cleavage along the axis of the rock particle as seen in the Figure 1.4a and in Figure 1.4c (Donovan, 2003).

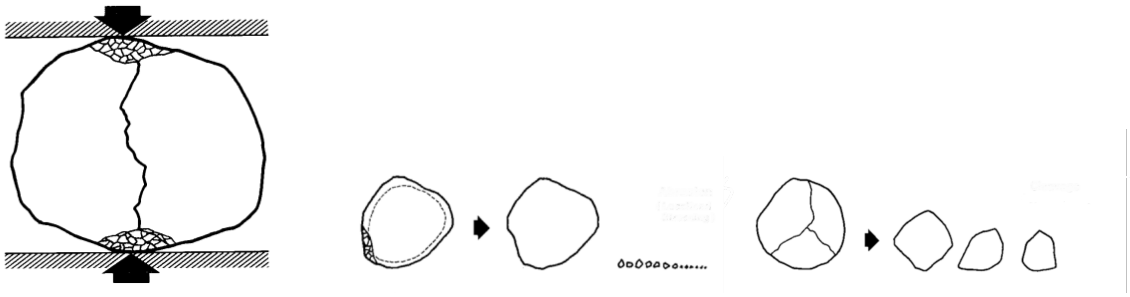

(a) Rock Failure During the Crushing Process (b) Abrasion Fracture (c) Cleavage Fracture

Figure 1.4: Rock Failure During the Crushing process (Donovan, 2003)

The failed-rock fragments drop down the crushing chamber and undergo continuous nipping until they drop out when their sizes are less than the discharge opening at the bottom of the chamber. The increasing stroke at the bottom part of the swing jaw is necessary to allow crushed rocks to drop and avoid choking the crusher.

1.2 Problem Statement

The techniques of stone crushing in developing countries are either via very expensive imported machines tools which cannot be afforded by the majority of middle-class entrepreneurs or the manual tools whose productivity is too low to make business sense. These problems have discouraged potential entrepreneurs from engaging in construction businesses and denied the affected countries a chance to develop themselves to a level of self-dependence. For instance, in Kenya, an 8 tonnes per hour, 16 HP imported crusher currently costs Ksh. 1.5 million (Mwafrika, 2018). Meanwhile, a research suggested that it takes a hardworking man 3 weeks to produce 7 tonnes of crushed rocks using the manual means (Munyasi & Oduori, 2012).

Typically, the construction industry is largely composed of few, centralized large-scale mechanized stone crushing businesses and majority small-scale manual rock crushing businesses. The former is costly to hire or purchase hence only a few people can afford it. Increased growth in the construction industry has led to the increase in prices charged for the large-scale mechanized rock crushers. This has led to the mushrooming of small-scale manual crushing enterprises where people use hammers and anvil for the job. Manual crushing jobs are cumbersome, dangerous, and give low-quality products as well as low output.

Furthermore, the existing crushing machines are manufactured elsewhere in the developed countries only to be imported into developing countries. Consequently, such machines are only beneficial to the economies of the developing countries at their end-use point. Such countries do not benefit at the stages of machine design, fabrication, and assembly.

Moreover, the mechanised jaw crushers grapple with the problem of inadequate crushing forces and inefficient motion transmission leading to inefficient crushing. This is because the crushing mechanism designs are neither optimised for force nor

motion transmission but rather are created using experienced estimations. One way of force and motion optimisation is by choosing optimum lengths of the crusher components as outlined by Zhao et al. (La-la, Zhong-bin, & Feng, 2008).

Design optimisation of a single-toggle jaw crushing mechanism will ensure that the small-scale entrepreneurs acquire a high production, cheaper, safer, more profitable, less energy intensive, easily portable, and locally designed crushing equipment. This will be a big step towards technology transfer which is beneficial to the developing economies.

1.3 Objectives

1.3.1 General Objective

The main objective of this study is to optimise motion and force transmission in the design of a single-toggle jaw crushing mechanism.

1.3.2 Specific Objectives

To achieve the above objective, the following specific objectives will be accomplished:

1. To optimise the crushing jaw motion for the single-toggle jaw crushing mechanism.
2. To perform static force optimisation of the single-toggle jaw crushing mechanism.
3. To perform dynamic force optimisation of the single-toggle jaw crushing mechanism.

1.4 Justification

The demand for aggregates worldwide today is very high. In Kenya, the government and the private sectors are investing heavily in infrastructure projects such as railway lines, roads, bridges and housing units which are all dependent on aggregates. Traditionally, sand and gravel are the main components of aggregates; however, due to the depletion of these resources at the mines, the modern source of aggregates is quarry rocks which are crushed to produce small-sized manufactured sand. Also, while naturally occuring sand and gravel are ungraded, the jaw crushers produce graded manufactured sand which is of higher quality.

The world as an estimated sand and gravel resource of 12 trillion tonnes each. This resource is at risk due to the accelerated extraction and use occassioned by high demand for the same. Nevertheless, the world still possesses 125 trillion tonnes of crushable stones and 42 million tonnes of quality stones that can be used to produce cut stones (Sverdrup, Koca, & Schlyter, 2017). Therefore, the world has adequate rocks to generate aggregates to reduce pressure on the naturally occuring aggregates. Crushed rocks would also help in conservation of river ecosystems and coastal beaches which have been the main natural sources of sand and gravel.

Efforts to achieve an optimised single-toggle jaw crusher will help to overcome the inefficiency problem experienced in the jaw crushers in the market thus leading to increased crushing capacity. Since a medium scale crusher is targetted, it will also reduce the cost implication of mechanised crushing and encourage MSMEs which are the main building blocks for industrialization in Kenya and are core to the accomplishment of the Vision 2030 (Wairimu, 2015). The optimised crusher will help the mining and quarrying industry from overrelying on manual crushing techniques which have been found not only unsafe but also tiresome, less productive and less profitable.

CHAPTER TWO

LITERATURE REVIEW

2.1 Overview

Jaw crushers are essential equipment in quarrying and mining industries used for primary crushing especially for the production of aggregate materials required in construction of buildings and other infrastructure. The single-toggle jaw crusher is the most common of these crushers. The productivity of the crushers is measured in terms of their capacity which is, the mass or volume of material crushed per unit operation time. The capacity is dependent on the ability of the crushing mechanism to supply force and motion in the direction of crushing. An adequate supply of these two critical parameters results in higher productivity and vice versa. However, most mines and quarries are grappling with the problem of the jaw crushers not supplying enough crushing force and motion leading to low efficiency and high energy consumption (La-la et al., 2008). This chapter presents a review of the research works that have been carried out to improve the functionality of a single-toggle jaw crusher mechanism.

2.2 Kinematic Analysis of Single Toggle Jaw Crusher Mechanism

Kinematic analysis of the single-toggle jaw crusher is important since the comminution process is achieved through the special motion of the mechanism. In kinematics, mathematical models are formulated for the position, velocity, and acceleration analysis of the mechanism (Rusiński, Moczko, Pietrusiak, & Przybyłek,

2013). The jaw crusher can be modelled as a planar four-bar mechanism with the coupler as the output link. The frame is the fixed link, the eccentric shaft is the short crank, the swing jaw is the coupler, and the toggle plate is the rocker. In modelling the jaw crusher as a four-bar linkage, the mechanism is represented as shown in Figure 2.1 where r_2 is the length of the crank, r_3 the length of the coupler, r_4 the length of the rocker and r_1 is the length of the fixed link.

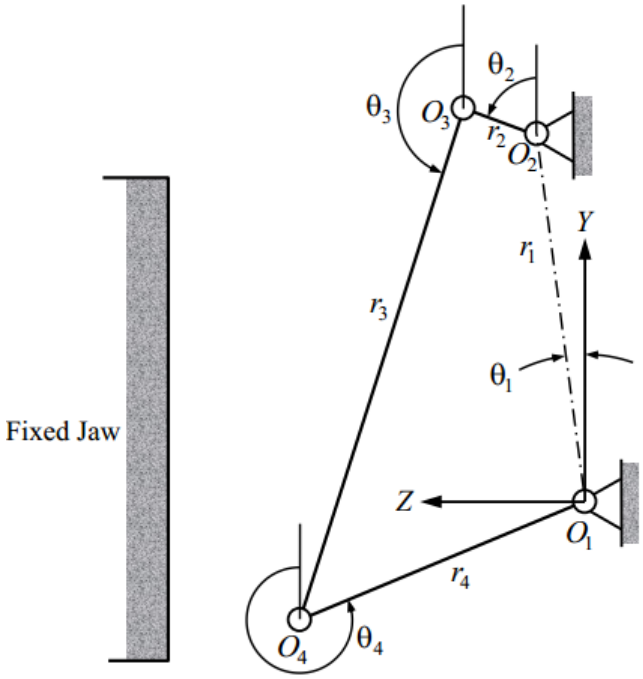

Figure 2.1: Model of the jaw crusher as a crank-rocker mechanism (M. Oduori et al., 2015)

In this model, some assumptions are made to enable analysis of jaw crusher kinematics using existing laws of mechanisms. Firstly, the links are assumed to be completely rigid and therefore do not deform during the mechanism motions. Secondly, the mechanism is closed for all cycles of operation of the jaw crusher. This allows the bar lengths to be taken as vectors in a closed loop system.

Cao et al.(Cao, Rong, & Yang, 2006) used the PE 400 × 600 jaw crusher model to provide a detailed description of the swing jaw movement, study the crushing force

distribution and relate the two to jaw plate wear. The numbers 400 and 600 indicate the gape and width of the plates respectively. The gape is the space between the jaws at the feeding point. It concluded that the vertical motion of the swing jaw was responsible for jaw wear. The study gives great insight into the kinematics of the single-toggle jaw crusher by revealing the double motion of the swing jaw during the crushing process. However, it only concentrated on the contribution of the vertical motion towards wear and did not focus on the horizontal stroke which is the key source of crushing power.

Garnaik (Garnaik, 2010) did a detailed description and interpretation of the motion of the swing jaw in order to understand the relationship between jaw movement and forces. This study added to the knowledge of motion of the swing jaw of the single-toggle jaw crusher mechanism by relating it to crank motion. However, these findings cannot be used to evaluate the efficiency of motion transmission from the crank to the swing jaw.

Oduori et al. (M. Oduori et al., 2015) presented a study of the analytical kinematic analysis of the single-toggle jaw crusher mechanism aimed at obtaining equations to define the motion of any point on the swing jaw. The study modelled the crusher as a planar mechanism of the crank-rocker type with the output link being the swing jaw. The position, velocity, and acceleration equations were derived from first principles based on the vector-loop closure and differential calculus methods. Though the study provided a proper description of the motion of the swing jaw, it did not provide a motion property which can be used to compare different models of the single-toggle jaw crusher. This could be essential in order to rate the motion efficiency of the crushing jaws in different mechanisms.

Luo and Li (Luo & Li, 2012) determined the characteristic value of the moving jaw plate for use in a multi-objective capacity optimisation of the double toggle jaw crusher. The study derived equations for the bottom most point on the swing jaw

and used them to calculate the vertical and horizontal stroke whose ratio gave the characterisitc value. The study provides novel equations for the kinematic analysis of a double toggle jaw crusher. Though the analysis gives good insight into the analytical study of the jaw crusher, the equations developed cannot be applied to a single toggle jaw crusher.

Zhao et al. (La-la et al., 2008) used the characteristic value of the bottom most part of the swing jaw as well as the transmission angle to optimise a combined crusher consisting of both a single-toggle jaw crusher and a toothed roll crusher in an evolutionary optimisation process. Transmission angle is the angle between coupler and rocker in a four bar mechanism while the characteristic value is the ratio of the vertical-to-horizontal motions of the swing jaw lowest point. The characteristic value obtained is independent of the actual link lengths since all lengths are taken relative to the rocker length; this makes the model more universally acceptable. However, the use of transmission angle in the model introduces inaccuracies as this parameter is only applicable to mechanisms whose output is the rocker.

Zhang et al. (L. Zhang, Shen, Cao, & Lv, 2012) studied the characteristic value of the jaw crusher computationally using virtual prototype technology. The study conducted a design of experiments in MacNeal-Schwendler Corporation Automated Dynamic Analysis of Mechanical Systems (MSC ADAMS) comprising of four factors each with four levels. The factors were the crank, coupler, rocker and toggle plate oscillation angle. This study provides a special kinematic study of the jaw crusher based on computational methods as well as optimisation based on design of experiments . However, the study results are limited by the exclusion of the fixed link amongst the factors.

2.3 Force Transmission in a Single Toggle Jaw Crusher

As earlier stated, the single-toggle jaw crusher applies both compressive and shear crushing forces on the feed material. Most of the crushing is achieved via compression, though the shear increases the throughput of the mechanism. Several authors have studied the quantification of the force transmission in the single-toggle jaw crusher. One measure of force transmission is the mechanical advantage. Traditionally, mechanical advantage of a four bar planar linkage is presented in the form of the transmission angle (Doane, 2016; Myszka, 2012; Rattan, 2009). Nevertheless, the transmission angle technique is not suitable for the single-toggle jaw crusher design whose output link is the coupler and not the rocker as is conventional.

Another measure of the transmission efficiency is the characteristic travel of the moving jaw plate. The characteristic travel is a kinematic property and is defined as the ratio of the vertical to horizontal motion of the lowest point of the swing jaw (Luo & Li, 2012). While the horizontal motion is responsible for crushing the feed material, the vertical motion magnifies the abrasion of the jaws. Reducing the value of the characteristic travel improves production and crushing ratio and diminishes energy consumption and abrasion (La-la et al., 2008). From experience, the characteristic travel of a good jaw crusher design should range from 1.5 to 2.5 (La-la et al., 2008; Luo & Li, 2012; L. Zhang et al., 2012). Since this entire range is greater than unity, the vertical travel is always greater than the horizontal travel and this helps to enhance the throughput of the machine. A ratio lower than 1.5 could mean a decrease in the throughput of the mechanism while one higher than 2.5 could result in excessive wear through abrasion as a result of too much vertical motion of the crushing jaw.

Huang et al. (Huang, Lei, & Wang, 2011) created a jaw crusher model using

SOLIDWORKS and analysed it in MSC ADAMS software to investigate both the transmission angle and the characteristic travel. The research emphasized on the need for the horizontal travel to be large enough to achieve good feeding effect for crushing. It also focussed on making the vertical travel small enough, gradually decreasing from the top of the swing jaw, in order to reduce abrasion, reduce overgrinding and offer smooth material discharge. In addition, the authors shed light on the need to avoid having a transmission angle that is too high or too low, both cases of which reduce transmission efficiency. High transmission angles increase power consumption and jaw linings abrasion and low transmission angles give low transmission efficiency. Nevertheless, the model used in the study had inferior characteristic values and unsuitable transmission angles.

Oduori et al. (M. Oduori et al., 2015) proposed a characteristic mechanical advantage (MA) for comparison of static forces in single-toggle jaw crushers. The authors derived the MA from first principles of static equilibrium. The mechanical advantage was a function of the coupler torque and the input crank torque. The index developed was a dimensionless measure of the mean value of force transmission over the active stroke of the moving jaw. However, this index was for static force transmission only and did not consider dynamic forces arising from acceleration. Furthermore, the index ignored the idle stroke during which, power input still persists for the retraction of the jaw.

Lin and Chang (C. C. Lin & Chang, 2002) also proposed a force transmission index (FTI) as a measure of the quality of transmission between the input and output links especially for complex linkages with multiple degrees of freedom. The FTI proposed was a dimensionless quantity ranging from 0 to $+\infty$ and was the result of the absolute value of the product Effective Force Ratio (EFR) and the loading moment of unity intensity, and Mechanical Advantage (MA). While the MA measured the performance of the input link, the EFR measured the performance of the output link. Force transmission index (FTI) is applicable to all four-bar mechanisms regardless

of the choice of input and output link, unlike the case of the transmission angle. The index developed was, however, only applicable to static force transmission. Also, the load was assumed to be unity which is not always the case (C. C. Lin & Chang, 2002).

Golikov and Timofeev (Golikov & Timofeev, 2018) studied the force transmission problem in a jaw crusher by considering the factors affecting its capacity. The authors outlined the capacity of the crusher as being dependent on the crusher design as well as the motion of the swing jaw. A mathematical model was developed which stated that the capacity of the jaw crusher is directly proportional to the average compression stroke and inversely proportional to the crushing ratio. The final expression obtained in the study is useful in appreciating the importance of operation mode parameters to the capacity of the jaw crusher and for comparison of different designs of jaw crushers. However, the researchers only relied on semi-empirical and empirical equations which could only give approximations (Golikov & Timofeev, 2018).

Luo and Li (Luo & Li, 2012) performed a comprehensive study on the optimisation of a double toggle jaw crusher mechanism. The authors conducted multi-objective optimisation of the crusher which consisted of a function for the reduction of the characteristic value of the moving jaw(F_1), function for the maximization of the crusher capacity(F_2), function for the minimization of the outlet width (F_3) and function for the reduction of the jaw crusher size (F_4). All these functions formed the multi-objective function shown in Equation 2.1 (Luo & Li, 2012).

$$\min \ F(X) = W_1F_1(X) + W_2F_2(X) + W_3F_3(X) + W_4F_4(X) \tag{2.1}$$

where W_1, W_2, W_3, and W_4 are arbitrary weighting factors.

This study was very important in understanding some of the crucial constraints

required in the optimisation of the jaw crusher. These included the constraints on the transmission angle, the nip angle between the fixed jaw and moving jaw, the horizontal stroke on both the topmost and bottommost points, and the Grashof's law. Nevertheless, the major shortcoming in the research was the use of arbitrary weighting factors for the various objective function elements considered.

Zhao et al. (La-la et al., 2008) improved the capability of a combined crusher (both roller and jaw crusher) by utilising Genetic Algorithm (GA) to optimise both the transmission angle and the characteristic travel. The length of the crank was assumed to be unity and GA was used to optimise a multi-objective function encompassing both the characteristic ratio and transmission angle. The study was beneficial as it illuminated into the importance of GA in engineering optimisation. It also showed the different constraints which should be considered during the optimisation of the single-toggle jaw crusher. In addition to the constraints highlighted by Luo and Li (Luo & Li, 2012), this study includes others such as upper and lower limits of the design variables and the acceptable range of the characteristic travel. Nevertheless, the optimisation considered the transmission angle as part of the factors to be optimised which meant that only one value of the angle was obtained. Therefore, such a mechanism is not practical since the transmission angle is bound to change during the revolution of the crank. Furthermore, the study was also based on arbitrary choice of weighting factors for the multi-objective optimisation. In addition, the crusher in the study was a combined crusher thus the results cannot directly be applied to the single-toggle jaw crusher.

Zhang et al. (L. Zhang et al., 2012) conducted a Design of Experiments (DOE) study on the optimisation of the travelling characteristic of the single-toggle jaw crusher. In the study, a virtual prototype of the jaw crusher model PE 1500 $\times$ 1800 was developed in MSC ADAMS and subjected to an orthogonal factorial experiment design with four variables being studied. This study provides a special perspective of the optimisation of the jaw crusher using the DOE. Nevertheless, it is worth noting

that this study did not consider the effect of the fixed link on the travel characteristic. In addition, the study had the oscillation angle as one of the variables while the angle itself is a function of the lengths of the links in the mechanism. The angle is bound to change as the crank rotates and thus does not suffice to be picked as a design variable. It would, therefore, be prudent to carry out a similar study including all the links of the mechanism as design variables and excluding the oscillation angle so as to determine the effect of the mechanism design on its efficiency and capacity.

2.4 Application of Optimisation Algorithms in Jaw Crusher Mechanisms

Engineers have often resorted to learning from nature on how to deal with complex problems. Evolutionary Algorithms (EA) are engineering search techniques that imitate natural evolution to obtain the best solution to a problem based on a desired target. They are iterative and stochastic processes which operate on an initially high population and through constant sharing of fitness information achieve the best suited individual in the population; this process is called optimisation. In jaw crusher and related mechanisms, there are two common EA techniques used in optimisation namely genetic algorithm and particle swarm optimisation.

2.4.1 Genetic Algorithm (GA)

Genetic Algorithms are search and optimisation techniques that rely on the concept of natural selection. As is the case in nature, the fittest population is selected for continued survival but the unfit one is eliminated. The initial steps of the GA involve generation of a random population of possible solutions. The fitness of each member of the population is calculated based on the objective function and used as a rating criteria to select fit parents. Three natural genetic operators namely reproduction, crossover and mutation are applied to the fit population to create a new population

which forms the second generation. The three operators are applied successively through several iterations until the stopping criteria is met. At this point, the fit population and the optimal value of the objective function are produced (Sivanandam & Deepa, 2008) . Figure 2.2 shows a flowchart of the GA process.

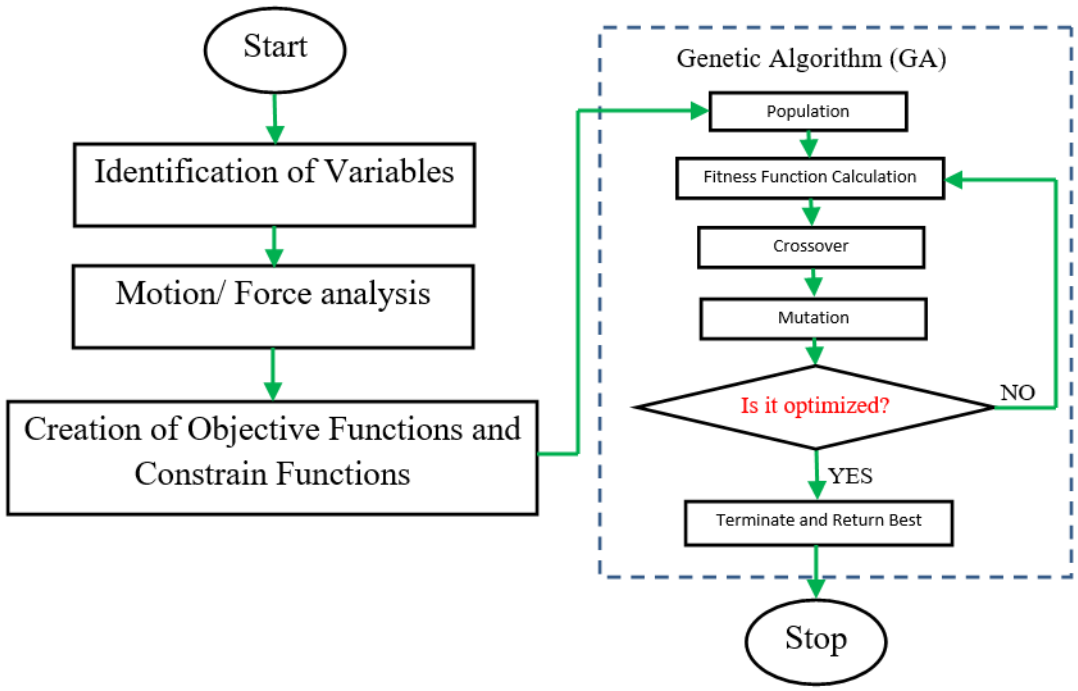

Figure 2.2: Flowchart showing the GA process (Bozorg-Haddad et al., 2017)

Genetic Algorithm acts on the objective function and not its derivative as is the case with gradient-based techniques. This is helpful as the algorithm can be applied to functions of continuous and discrete nature. It does not require knowledge of the problem structure and thus makes it suitable for dealing with functions which are non-linear, non-differentiable and noisy (Fidanova, 2013). Genetic Algorithm also performs better in terms of information sharing and convergence to the global solution. In GA, the information is shared amongst all the possible solutions in the population. In the crushing industry, Svedensten (Svedensten & Evertsson, 2005) used genetic algorithm for the optimisation of a crushing plant model using the

total gross profit as the cost function. Zhao et al. (La-la et al., 2008) performed a multi-objective study to optimise a combined roller-jaw crusher using genetic algorithm. Zhangfeng et al. (Zhangfeng et al., 2015) applied multi-objective genetic algorithm to the optimisation of both motion and structural parameters of a compound pendulum jaw crusher. Lee (Lee, 2012) applied genetic algorithm to the product and energy optimisation of compressive crushing of various rock materials. Genetic algorithm was also used by Asbjornsson (Asbjornsson, 2015) for the optimisation of the eccentric shaft speed to minimize recirculating materials for multi-stage comminution systems. Elsewhere, GA has been coupled with Differential Evolution (DE) for path synthesis of a four-bar mechanism (W. Y. Lin, 2010). Laribi et al. (Laribi, Mlika, Romdhane, & Zeghloul, 2004) augmented GA with a fuzzy logic controller for boundary adjustment in path generation of a four-bar mechanism.

2.4.2 Particle Swarm Optimisation (PSO)

Particle Swarm Optimisation is an evolutionary search algorithm to solve engineering problems based on the concept of bird flocking and behaviour of a swarm of insects. Birds and insects move in groups and continually communicate with each other to get best positions for food and protection giving them greater capability of survival.

Mu et al. (Mu, Lio, Li, Deng, & Huang, 2013) performed vibration signal extraction in a double cavity jaw crusher using a hybrid algorithm Differential Evolution Particle Swarm Optimisation (DEPSO). McDougall and Nokleby(Mcdougall & Nokleby, 2008) used PSO for the synthesise of a general purpose Grashof's mechanism. Wang et al. (Wang, Qin, Zhang, & Yang, 2012) optimised the four-bar linkage of a hydraulic support via an improved particle swarm optimisation (IPSO). Nedic et al. (Nedic, Prsic, Dubonjic, Stojanovic, & Djordjevic, 2014) relied on PSO to tune 24 parameters of a cascade controller in a 6 DOF parallel robot platform.

Although an evolutionary algorithm like the GA, PSO does not possess genetic

operators such as mutation and crossover making is suscetible to local minima points. Information sharing in PSO is one-way, from the best solution to the rest of the swarm. Particle Swarm Optimisation (PSO) converges fasters and requires definition of fewer parameters compared to other evolutionary computational techniques such as GA. It enjoys great preference in search problems involving high DOFs (Nedic et al., 2014; Sivanandam & Deepa, 2008).

Comparing the two EAs discussed above, the GA was selected for optimisation in the present study for a number of reasons. First, GA has superior information sharing systems as opposed to PSO where the information path is one way with the best solution in each iteration giving information to the others. Genetic Algorithm (GA) thus avoids the hurdle of being locked in a local minima (Panigrahi, Abraham, & Das, 2010). Furthermore, GA has the added advantage of availability of its commercial version as a toolkit in MATLAB software unlike PSO.

2.5 Summary of Research Gaps

From the literature reviewed, the following were the gaps identified:

1. Though research into the kinematics of the single-toggle jaw crusher has been done, little attention has been directed to connect the same to motion optimisation in order to improve the crusher efficiency.

2. Dynamic analysis of the single-toggle jaw crusher mechanism has had little focus from researchers. The effect of moving jaw acceleration has largely been understudied.

3. Most researchers have relied on the use of arbitrary weighting factors in the creation of their objective functions with little emphasis on the criteria to determine their values.

4. Several researchers have included the transmission angle as a variable in the

objective functions yet the same is a function of the link lengths.

This research will aim at addressing the gaps highlighted above.

CHAPTER THREE

METHODOLOGY

3.1 Overview

This chapter outlines the methodology used to achieve motion and force optimisation of a single-toggle jaw crusher. In each case, the optimisation process involved the derivation of mathematical objective functions which measure the efficacy of either motion or force transmission. The objective functions were fed into MATLAB GA tool and the optimum dimensions of the crusher model obtained. The results in each case were analysed to understand the behaviours of optimised jaw crusher models. Furthermore, the influence of the length of each of the crusher model links was determined.

3.2 Motion Optimisation

Motion in a single-toggle jaw crusher is closely related to the output capacity which is defined as the volume swept by the swing jaw. The volume is a product of travel area of the moving jaw and the width of the crusher. For a fixed crusher width, motion optimisation translates to capacity optimisation. In this study, optimisation aimed at maximising the crushing travel. The optimisation process requires an objective function which is to be either minimized or maximized. The objective function in this section is based on motion performance characteristics of the single-toggle jaw crushing mechanism model.

The single-toggle jaw crushing mechanism can be modelled as a four-bar mechanism of the crank-rocker type with the eccentricity as the crank, the swing jaw as the

coupler, the toggle plate as the rocker and the frame as the fixed link. Figure 3.1 shows a schematic representation of the four bar mechanism. The link AB is the crank, BC is the coupler, CD is the rocker, and AD is the frame.

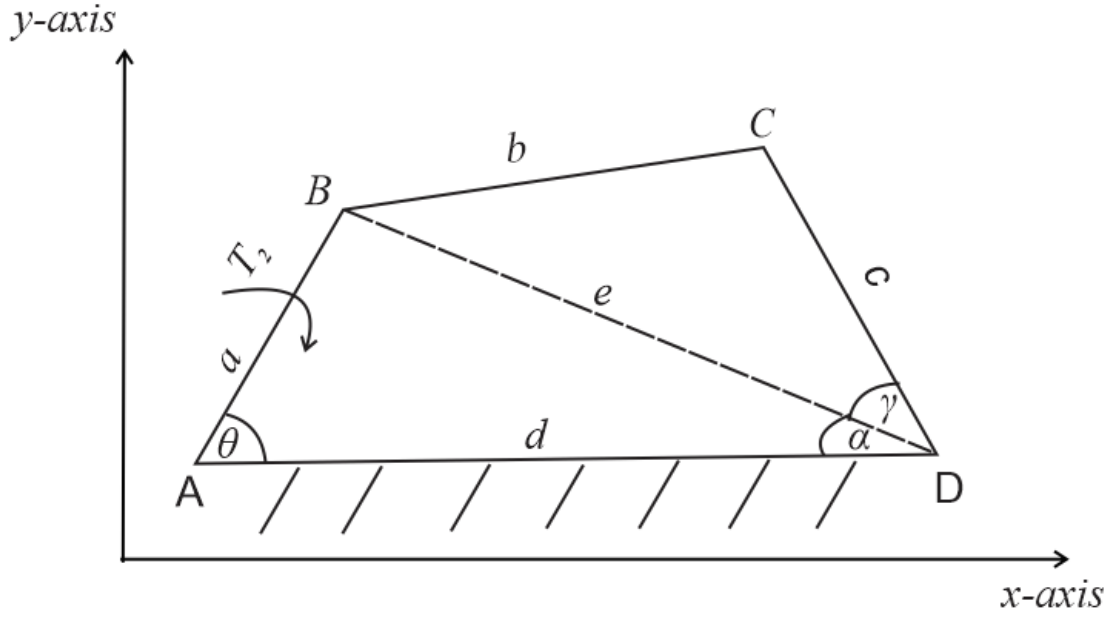

Figure 3.1: Schematic of the jaw crusher four bar mechanism

The positions of points B and C in the Cartesian plane were determined as functions of the angle θ and lengths of the links a, b and c. Point A was taken as the reference point with coordinates $(0, 0)$. Point D was a function of length d only. The position vector of point B was given by,

$$\overrightarrow{B} = a\ \cos\theta\ \hat{i} + a\ \sin\theta\ \hat{j} \tag{3.1}$$

where θ is the crank angle, a is the crank length, $\hat{i}$ and $\hat{j}$ represents unit vector in the x and y directions respectively.

Meanwhile, point D was a fixed point on the frame whose position only depended on the frame length d. It was assumed that the frame was not inclined and the angular

position of point D from the reference A was 0^0. The assumption is valid since, in most cases, the angular inclination is usually very small. For instance, in the popular Cao et al. design (Jinxi, Zhiyu, Guopeng, Xingfu, & Shichun, 2007), the inclination is 3.18^0. Therefore, the positional vector for point D was,

$$\overrightarrow{D} = d\ \hat{i}. \tag{3.2}$$

Point C was determined via three intermediary parameters namely, the diagonal e, the angle α in the $\Delta\ ADB$, and the angle γ in the $\Delta\ BDC$. The diagonal e as part of $\Delta\ ADB$ was written as,

$$e^2 = a^2 + d^2 - 2ad\cos\theta. \tag{3.3}$$

With length e already defined, the value of angle α was determined using the sine rule as shown,

$$\alpha = \sin^{-1}\left[\frac{a\sin\theta}{e}\right]. \tag{3.4}$$

On the other hand, the value of angle γ was calculated using the cosine rule as

$$\gamma = \cos^{-1}\left[\frac{e^2 + c^2 - b^2}{2\ ec}\right]. \tag{3.5}$$

Then the vector for point C was evaluated by

$$\overrightarrow{C} = \{d - c(\cos(\alpha+\gamma))\}\hat{i} + \{c\sin(\alpha+\gamma)\}\,\hat{j} \tag{3.6}$$

Crushing in a jaw crusher is achieved by the action of the entire swing jaw thus the

motion of all points on the jaw is important. The motion was evaluated in terms of travel range as the swing jaw moved towards and away from the swing jaw. A crank speed of 36 rad/s was adopted. The jaw was discretized into unit-spaced points whose travel was to be investigated. The total travel of jaw points was taken as the area under the graph of range of travel against the different points on the jaw. This travel was illustrated by using dimensions of a typical PE 400 $\times$ 600 single toggle jaw crusher given in Table 3.1.

Table 3.1: Dimensions of a typical jaw crusher (Cao et al., 2006)

Link	**Crank**	**Coupler**	**Rocker**	**Frame**
Length (mm)	12	1085	455	817

Shearing travel and crushing travel for the typical jaw crusher were as shown in Figure 3.2. The length of points on the swing jaw was measured from the top.

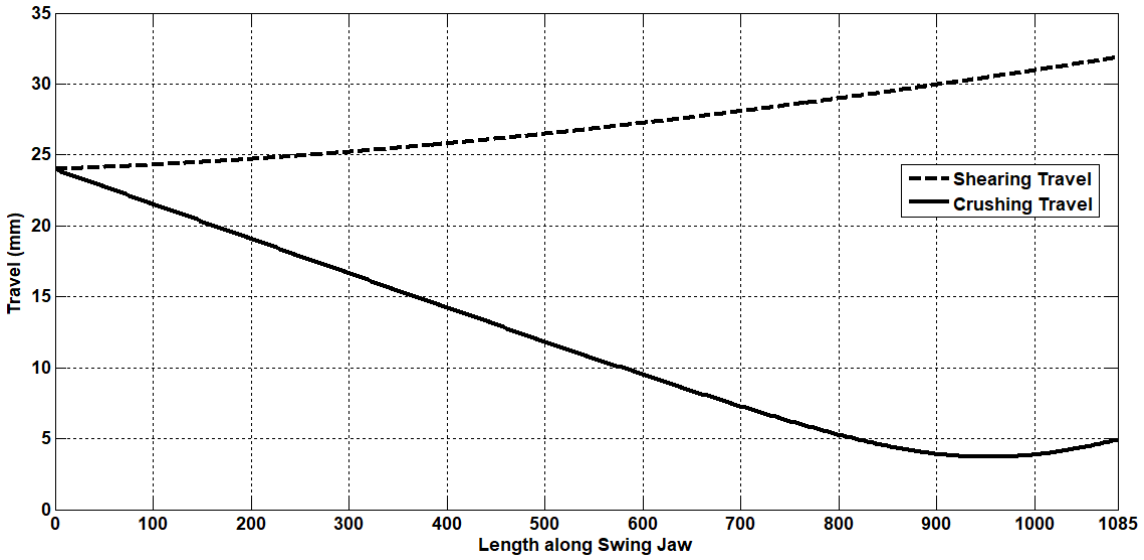

Figure 3.2: Shearing and crushing travels of swing jaw points

From Figure 3.2, the area under the shearing travel line became the shearing area while that under the crushing travel line became the crushing area. One way to achieve optimisation was to maximise the amount of crushing motion for all points

on the swing jaw. Alternatively, optimisation could mean maximisation of the crushing-shearing ratio. In this study, motion optimisation took the two routes. Each of them had a different objective function. The two objective functions were formulated as in the two sections below. This method provides a novel criteria for evaluating the motion transmission performance of a single-toggle jaw crusher by determining the range of total crushing travel and shearing travel for all points of the swing jaw of a single-toggle jaw crushing mechanism. High crushing travel and low shearing travel would mean better perfomance of the crusher.

3.2.1 Objective Function Based on both Crushing Travel and Shearing Travel

The first objective function was based on the ratio of total shearing to total crushing travels for several points on the swing jaw. The shearing-crushing ratio was

$$Y_1 = \frac{A_X}{A_Y}, \tag{3.7}$$

where, y_1 is the shearing-crushing ratio, A_X is the area under shearing travel graph,and A_Y is the area under crushing travel graph.

Through optimisation, it was desired that the mechanism obtained would minimise the shearing-crushing ratio.

3.2.2 Objective Function Based on Crushing Travel Only

The second objective function was based on the crushing travel only and bore the second crusher motion measurement characteristic. The crush travel inverse was

$$Y_2 = \frac{1}{A_Y} \tag{3.8}$$

The process aimed at maximising the crushing area and disregarded the shearing area.

The two motion based objective functions were actualised using the GA solver in MATLAB. The MATLAB code for the two objective functions was as shown in Appendix A.

3.3 Force Optimisation

After motion optimisation, force optimisation was done to develop optimum jaw crusher designs which delivered the highest crushing force to the rocks being crushed. This section had two objective functions: static crushing force and dynamic crushing force. Both sections start with force analysis on the swing jaw of the jaw crusher from first principles. What follows are respective objective functions based on the crushing torque exerted onto the rocks by the moving jaw.

3.3.1 Static Crushing Force

Static force analysis was also carried out in MATLAB software. The analysis was based on the crank-rocker model of the jaw crusher. The ability of rocks to be crushed is determined by their fracture toughness. Fracture toughness represents material's ability to withstand crack propagation. Donovan (Donovan, 2003) established a strong correlation between fracture toughness and tensile strength for rocks crushed using jaw crushers. Therefore, fracture in rocks is caused by tension due to the application of compression loads. The main form of failure in rock crushing is cleavage fracture due to induced tensile stresses as rocks are ten times weaker in tension than compression due to naturally occuring cracks in the rocks. Compressive stresses tend to close the cracks thus strengthening the rocks; tensile stresses tend to open the cracks contributing to failure (Donovan, 2003).

In jaw crushers, the useful force that goes towards rock crushing is the applied

compressive force from the swing jaw which in turn induces tensile stresses in the rocks (Donovan, 2003). The compressive force, P_C, was taken to be perpendicular to the swing jaw. Also, the contribution of shear force P_S acting parallel to the swing jaw cannot be ignored since.

Granite was chosen as the rock to be crushed as it is the commonest igneous rock and is the most abundant material in quarries (Wills & Napier-Munn, 2006). According to Rumbarger (Rumbarger, 2003), for unconfined granite, the compressive strength is in the range of $103.4 - 138$ MPa while the shear strength is $12.4 - 18.6$ MPa. In both cases, the upper limit was used for force analyses. Therefore, the tensile strength of the rock was 138 MPa and the shear strength was 18.6 MPa. The two tranlated to a compressive force of $13.8b^2$ MN and a shear force of $1.86b^2$ MN where b was the length of the swing jaw. The breadth of the swing jaw was assumed to be a tenth of its length. Also, the compressive force was assumed to be concentrated at the centre of mass of the swing jaw.

In performing static force analysis, three external forces all applied at the center of mass of the coupler were considered namely, crushing force P_C, shearing force P_S, and weight of the rocks, F. An input torque, T_2, was provided to power the mechanism while an output torque T_3 was the torque responsible for crushing the stones. Angle θ was the crank angle, β was the coupler angle and φ was the rocker angle. Link 1 was the frame, link 2 was the crank, link 3 and link 4 was the rocker. The static force analysis model was as shown in Figure 3.3.

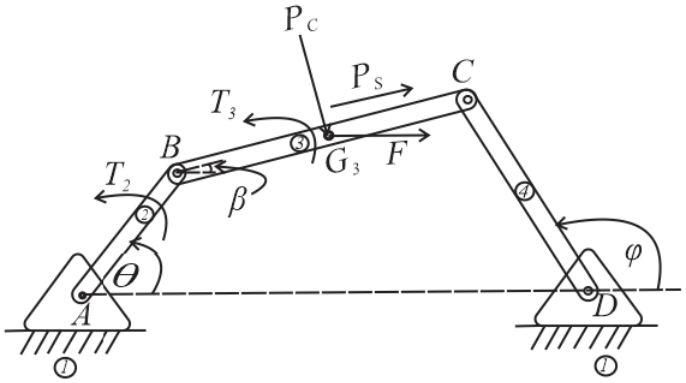

Figure 3.3: Static force model

The coupler was a three-force member composed of a resultant force $\overrightarrow{R}$ due to the three externally applied forces, internal force by link 2 on link 3 ($\overrightarrow{F_{23}}$) and internal force applied by link 4 on link 3 ($\overrightarrow{F_{43}}$). For concurrency, the three forces must intersect at a common point as shown in the free body diagram of the coupler in Figure 3.4. The lines of action (LOA) of the internal forces were thus determined as shown in Figure 3.4.

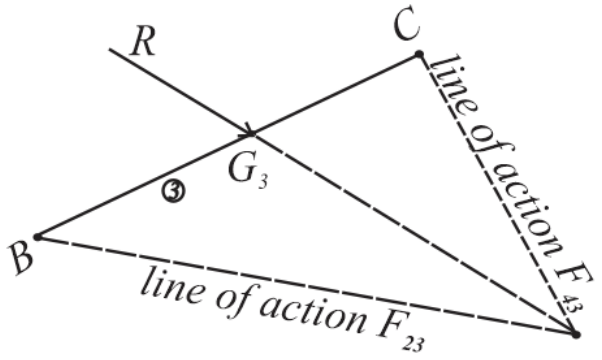

Figure 3.4: Free body diagram of the coupler

Here, $\overrightarrow{R}$ was the resultant of the three external forces, $\overrightarrow{P_C}$, $\overrightarrow{P_S}$, and $\overrightarrow{F}$. It was defined as

$$
\begin{aligned}
\overrightarrow{R} &= \overrightarrow{P_C} + \overrightarrow{P_S} + \overrightarrow{F} \\
\overrightarrow{P_C} &= P_C\Big\{\sin\beta\hat{i} - \cos\beta\hat{j}\Big\} \\
\overrightarrow{P_S} &= P_S\Big\{\cos\beta\hat{i} + \sin\beta\hat{j}\Big\} \qquad , \qquad (3.9) \\
\overrightarrow{F} &= F\hat{i} \\
\overrightarrow{R} &= \hat{i}\Big\{P_C\sin\beta + P_S\cos\beta + F\Big\} + \hat{j}\Big\{-P_C\cos\beta + P_S\sin\beta\Big\}
\end{aligned}
$$

With the forces on the coupler shown in Figure 3.4, the force polygon in Figure 3.5 was developed.

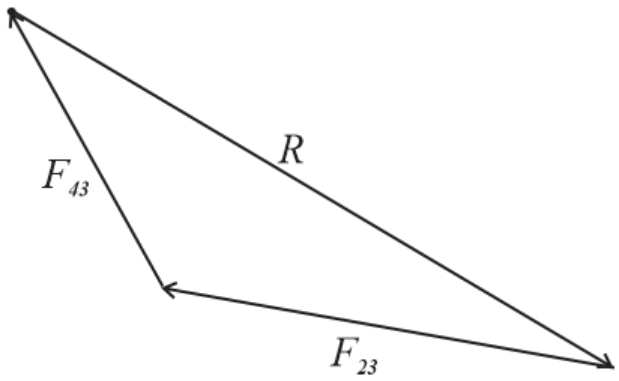

Figure 3.5: Force polygon for the coupler

For equilibrium of forces on link 3, Equation 3.10 was true.

$$\overrightarrow{F_{43}} + \overrightarrow{F_{23}} + \overrightarrow{R} = 0 \qquad (3.10)$$

Both $\overrightarrow{F_{43}}$ and $\overrightarrow{F_{23}}$ were known in direction but unknown in magnitude and could be written as

$$\overrightarrow{F_{43}} = F_{43}\left\{\cos\varphi\hat{i} + \sin\varphi\hat{j}\right\}$$
$$\overrightarrow{F_{23}} = -\overrightarrow{F_{43}} - \overrightarrow{R}$$
$$\overrightarrow{F_{23}} = \hat{i}\left\{-P_C\sin\beta - P_S\cos\beta - F - F_{43}\cos\varphi\right\} + \hat{j}\left\{P_C\cos\beta - P_S\sin\beta - F_{43}\sin\varphi\right\} \tag{3.11}$$

The magnitude of $\overrightarrow{F_{23}}$ was obtained by considering the crank link. A free body of the crank was as shown in Figure 3.6.

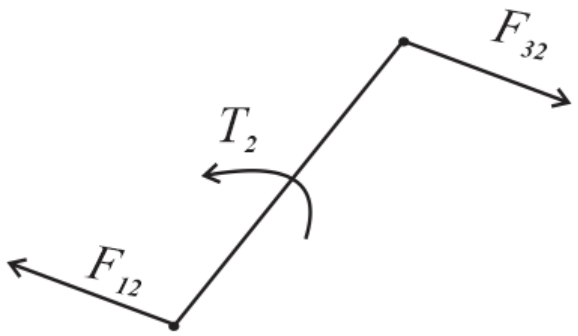

Figure 3.6: Free body diagram of link 2

.

In Figure 3.6, force $\overrightarrow{F_{12}}$ was the force applied by the frame on the crank while force $\overrightarrow{F_{32}}$ was the force of the coupler on the crank. The two forces were equal and formed a couple which was equivalent to the input torque, T_2 as shown by

$$\overrightarrow{T_2} = \overrightarrow{F_{32}} \times \overrightarrow{a} = -\overrightarrow{F_{23}} \times \overrightarrow{a}$$

$$\overrightarrow{T_2} = \left[\hat{i}\left\{F_{43}\cos\varphi + P_C\sin\beta + P_S\cos\beta + F\right\} + \hat{j}\left\{-P_C\cos\beta + P_S\sin\beta + F_{43}\sin\varphi\right\}\right]$$
$$\times \left[a\left\{\cos\theta\ \hat{i} + \sin\theta\ \hat{j}\right\}\right]$$

$$T_2 = a\left\{\sin\theta\left[F_{43}\cos\varphi + P_C\sin\beta + P_S\cos\beta + F\right] - \cos\theta\left[-P_C\cos\beta + P_S\sin\beta + F_{43}\sin\varphi\right]\right\} \tag{3.12}$$

where $\overrightarrow{a}$ was the length vector of the crank with magnitude a and force vector $\overrightarrow{F_{43}}$ was the force applied by the coupler on the crank whose magnitude was F_{43}

The magnitude of force $\overrightarrow{F_{43}}$ was obtained by

$$F_{43} = \frac{T_2 - a\left[P_C\cos(\theta-\beta) + P_S\sin(\theta-\beta) + F\sin\theta\right]}{a\sin(\theta-\varphi)} \tag{3.13}$$

Having obtained the magnitude of force $\overrightarrow{F_{43}}$, the value of the output torque, T_3 was determined by taking moments about point B, the joint between crank and coupler:

$$M_B = \overrightarrow{P_C} \times \overrightarrow{BG_3} + \overrightarrow{P_S} \times \overrightarrow{BG_3} + \overrightarrow{F_{43}} \times \overrightarrow{BC} + \overrightarrow{F} \times \overrightarrow{BG_3} + T_3 = 0 \tag{3.14}$$

where $\overrightarrow{BG_3}$ is the displacement vector for the length between crank-coupler joint and centre of mass of the coupler, $\overrightarrow{BC}$ is the displacement vector for the coupler length and T_3 is the output torque of the coupler.

The angles of the vectors in the moment equation were measured from a horizontal reference. The crushing force $\overrightarrow{P_C}$ made an angle (270+β), weight vector $\overrightarrow{F}$ was parallel to the horizontal and the internal force vector $\overrightarrow{F_{43}}$ was at an angle φ. The

shearing force $\overrightarrow{P_S}$, the length vectors $\overrightarrow{BC}$ and $\overrightarrow{BG_3}$ were parallel to the coupler which was at an angle β to the horizontal. These angles can be summarised as,

$$\begin{aligned}
\overrightarrow{P_C} &= P_C \angle(270+\beta) \\
\overrightarrow{P_S} &= P_S \angle\beta \\
\overrightarrow{BG_3} &= \frac{b}{2}\angle\beta \\
\overrightarrow{F_{43}} &= F_{43}\angle\varphi \\
\overrightarrow{BC} &= b\angle\beta \\
\overrightarrow{F} &= F\angle 0
\end{aligned} \tag{3.15}$$

where b is the coupler length.

With the assumption of uniform density for the link, the centre of mass for the coupler was taken to be at its centroid.The moment equation vectors were further expanded into their respective unit vectors in the $\hat{i}$ and $\hat{j}$ directions as,

$$\begin{aligned}
\overrightarrow{P_C} &= P_C \left[\cos(270+\beta)\hat{i} + \sin(270+\beta)\hat{j}\right] = P_C \left[\sin\beta\hat{i} - \cos\beta\hat{j}\right] \\
\overrightarrow{P_S} &= P_S \left[\cos\beta\hat{i} + \sin\beta\hat{j}\right] \\
\overrightarrow{BG_3} &= \frac{b}{2}\left[\cos\beta\hat{i} + \sin\beta\hat{j}\right] \\
\overrightarrow{F_{43}} &= F_{43}\left[\cos\varphi\hat{i} + \sin\varphi\hat{j}\right] \\
\overrightarrow{BC} &= b\left[\cos\beta\hat{i} + \sin\beta\hat{j}\right] \\
\overrightarrow{F} &= F\hat{i}
\end{aligned} \tag{3.16}$$

With the above definitions, the moment equation became,

$$\begin{aligned} M_B =& P_C[\sin\beta\hat{i} - \cos\beta\hat{j}] \times \frac{b}{2}\left[\cos\beta\hat{i} + \sin\beta\hat{j}\right] + F_{43}\left[\cos\varphi\hat{i} + \sin\varphi\hat{j}\right] \\ & \times b\left[\cos\beta\hat{i} + \sin\beta\hat{j}\right] + \left[F\hat{i}\right] \times \frac{b}{2}\left[\cos\beta\hat{i} + \sin\beta\hat{j}\right] + T_3 = 0 \end{aligned} \tag{3.17}$$

The result of the matrix cross products was

$$b\left\{\frac{F}{2}\sin\beta + \ F_{43}\sin(\beta - \varphi) + \frac{P_C}{2}\right\} + T_3 = 0 \tag{3.18}$$

Rearranging to get an expression for the magnitude of output torque, T_3,

$$T_3 = -\frac{b}{2}\left\{F\sin\beta + P_C + 2\ F_{43}\sin(\beta - \varphi)\right\} \tag{3.19}$$

Equation 3.19 is a novel equation which can be used for two purposes; first, it can be used as ac criteria to comapre the torque output of the single-toggle jaw crusher; it can also be used for optimisation as in Equation 3.20. In MATLAB, GA objective functions must be written in their minimisation forms. The objective function for static force optimisation was thus rewritten as,

$$Y_3 = \frac{1}{T_3} \tag{3.20}$$

where Y_3 was the static force optimisation function.

The objective function was used in MATLAB for static force optimisation. The MATLAB code for the implementation of function Y_3 was as shown in Appendix B.

3.3.2 Dynamic Crushing Force

Dynamic force analysis was also done using MATLAB software. Similar to the static force analysis case, the ratio of the two components of the dynamic force in the coupler-rocker joint was sought, that is, the ratio of the crushing component (horizontal direction) to the shearing component (vertical direction). To achieve this, the dynamic model shown in Figure 3.7 was used.

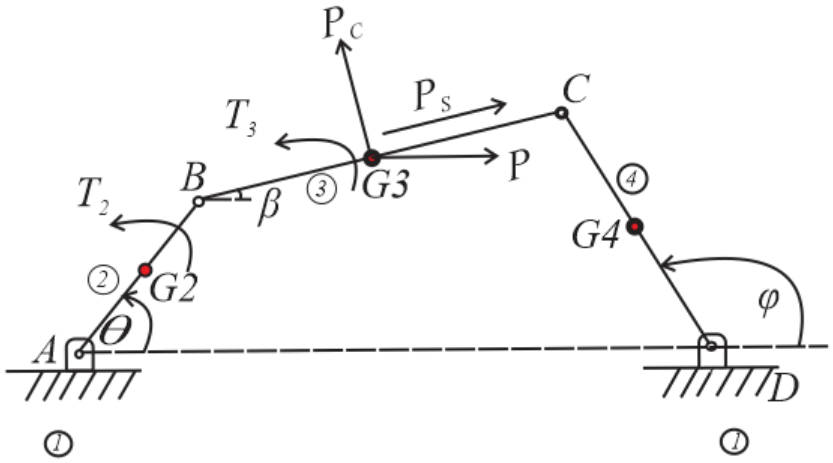

Figure 3.7: Dynamic model of the jaw crusher

In the model, link 1 was the frame, link 2 was the crank, link 3 was the coupler and link 4 was the rocker. Point A was the frame-crank joint, point B was the crank-coupler joint, point C was the coupler-rocker joint and point D was the rocker-frame joint. The points $G2$, $G3$ and $G4$ represented the centre of masses for the crank, coupler and rocker respectively. The crushing force P_C, shearing force P_S, and weight of the rocks, F were taken as point loads applied at the center of mass of the coupler. The mechanism was driven by an input torque, T_2, while an output torque T_3 aided in the stone crushing. Angle θ was the crank angle, β was the coupler angle and φ was the rocker angle.

According to the Newton's second law of motion (Stanisic, 2015), for dynamic

equilibrium of a rigid body, the net sum of static forces is equal to the inertia forces where the latter is a product of mass and acceleration of the body as shown by,

$$\begin{aligned} \Sigma F_x &= ma_x \\ \Sigma F_y &= ma_y \end{aligned} \tag{3.21}$$

where F_x is the net force acting on the body in the x direction, F_y is the net force acting on the body in the y direction, m is the mass of the body, a_x is the acceleration of the centre of mass of the body in the x direction and a_y is the acceleration of the centre of mass of the body in the y direction.

In rotary motion, according to Euler's equation (Waldron, Kinzel, & Agrawal, 2016), the resultant moment of forces acting on a body is equal to the inertial torque as in

$$\Sigma M = I\alpha \tag{3.22}$$

where M is the net moments about the centre of mass, I is moment of inertia of the body about the centre of mass, and α is the angular acceleration of the rotating body.

In the dynamic model, each link had the capability to translate in two directions, that is, x-direction and y-direction as well as to rotate in the z-direction. Therefore, two force equations and one moment equation were necessary to full define the motion of each link. Since the frame was fixed, only three links experienced motion and thus the entire mechanism was defined by nine motion equilibrium equations.

The nine equilibrium equations were developed from Figure 3.7, three for each link. The equations for the crank were guided by the free body diagram shown in Figure 3.8. Forces R_{12x} and R_{12y} were internal forces on the crank applied by the frame while R_{32x} and R_{32y} were applied by the coupler on the crank. The linear acceleration

of the centre of mass in the x and y directions were a_{G2x} and a_{G2y} respectively. The component m_2g represented the weight of the crank, angle θ was the crank angle, and T_2 was the input torque.

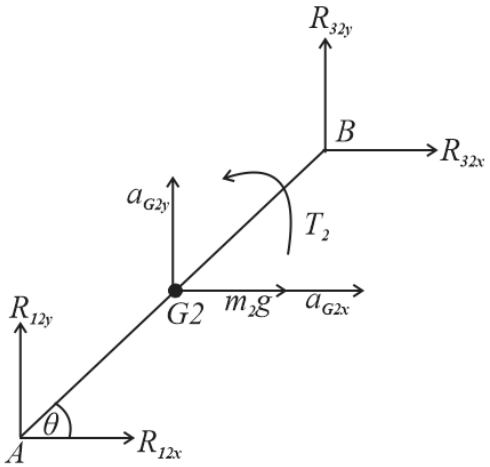

Figure 3.8: Free body diagram of the crank

For equilibrium in the x-direction, forces considered were the two internal forces in x-direction, one at each of the two joints as well as the weight of the link as shown by

$$\Sigma F_x = R_{12_x} + R_{32_x} + m_2 g = m_2 a_{G2_x} \tag{3.23}$$

In the y-direction, the internal forces R_{12y} and R_{32y} were taken into account in

$$\Sigma F_y = R_{12_y} + R_{32_y} = m_2 a_{G2_y} \tag{3.24}$$

In the z-direction, moment for all the forces and torque T_2 were considered. The moments were taken about the centre of mass of the crank,G_2 as follows,

$$\Sigma M = \frac{aR_{12_x}\sin\theta}{2} - \frac{aR_{12_y}\cos\theta}{2} - \frac{aR_{32_x}\sin\theta}{2} + \frac{aR_{32_y}\cos\theta}{2} + T_2 = I_2\alpha_2 \quad (3.25)$$

Meanwhile, the equations for the coupler were obtained using the free body diagram shown in Figure 3.9. Reaction forces applied by the crank were R_{23x} and R_{23y} and those applied by the rocker were R_{43x} and R_{43x}. External forces were the crushing force P_C, shearing force P_S and weight of the rocks F. The weight of the link was m_3g in the x-direction while the angle of the link with respect to the horizontal was β. Variables a_{G3x} and a_{G3y} were the accelerations of the coupler centre of mass in the x and y directions respectively.

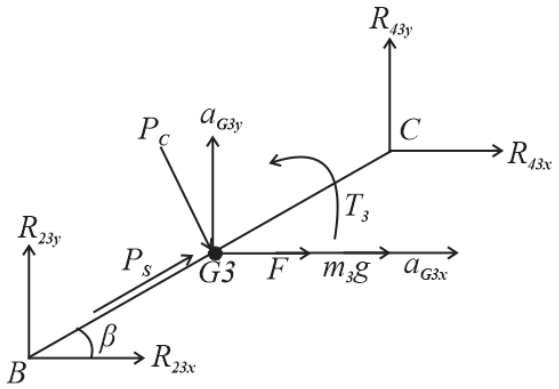

Figure 3.9: Free body diagram of the coupler

The equilibrium in the x-direction was evaluated by considering forces R_{23x} and R_{43x}, and components of P_C, P_S and F in the abscissa as in

$$\Sigma F_x = R_{23_x} + R_{43_x} + F + P_C\sin\beta + P_S\cos\beta + m_3g = m_3a_{G3_x} \quad (3.26)$$

The equilibrium in the y-direction was determined by considering forces R_{23y} and R_{43y}, and y-components of P_C, P_S and F as given by

$$\Sigma F_y = R_{23_y} + R_{43_y} - P_C \cos\beta + P_S \sin\beta = m_3 a_{G3_y} \tag{3.27}$$

Equilibrium in the axis of rotation was done by summing moments for all the forces about the centre of mass, adding the output torque T_3 and equating all that to the inertia torque of the coupler as in

$$\Sigma M = \frac{bR_{23_x}\sin\beta}{2} - \frac{bR_{23_y}\cos\beta}{2} - \frac{bR_{43_x}\sin\beta}{2} + \frac{bR_{43_y}\cos\beta}{2} + T_3 = I_3\alpha_3 \tag{3.28}$$

Finally, for the rocker the free body diagram was as shown in Figure 3.10. The rocker had no external forces, only reactions R_{34x} and R_{34y} from the coupler and reactions R_{14x} and R_{14y} from the frame in addition to the link weight $m_4 g$. The accelerations of the rocker centre were a_{G4x} and a_{G4y} in the x and y-axis respectively.

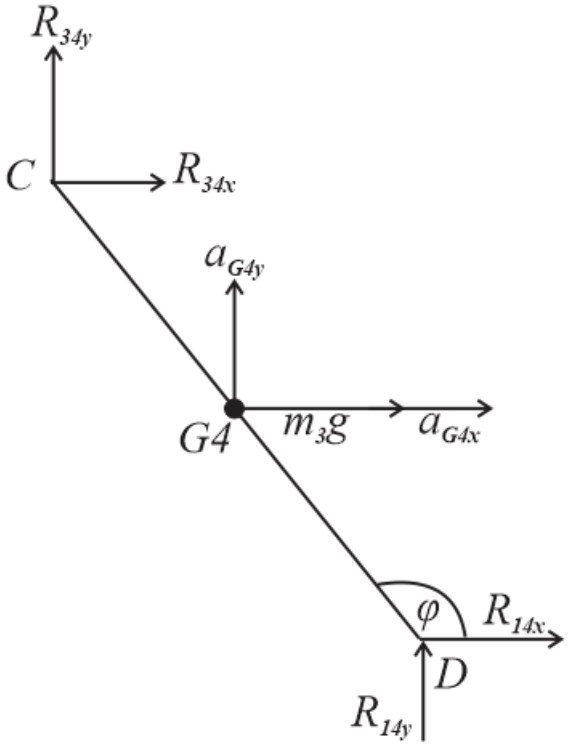

Figure 3.10: Free body diagram of the rocker

In the x-axis, the forces considered were R_{14x}, R_{34x} and rocker weight m_4g. The net result of these forces was equated to the inertia force in this direction as shown by

$$\Sigma F_x = R_{34_x} + R_{14_x} + m_4 g = m_4 a_{G4_x} \tag{3.29}$$

Forces in the y-axis included reactions R_{34y} and R_{14y} and the resultant equilibrium equation was

$$\Sigma F_y = R_{34_y} + R_{14_y} = m_4 a_{G4_y} \tag{3.30}$$

The equilibrium of moments and torques was determined by evaluating the moments of the four internal forces and equating to the inertial torque $I\alpha$

$$\Sigma M = \frac{cR_{34_x}\sin\varphi}{2} - \frac{cR_{34_y}\cos\varphi}{2} + \cdot\frac{cR_{14_x}\sin\varphi}{2} + \frac{cR_{14_y}\cos\varphi}{2} = I_4\alpha_4 \tag{3.31}$$

The acceleration components a_{G2_x}, a_{G2_y}, a_{G3_x}, a_{G3_y}, a_{G4_x}, and a_{G3_y} were obtained using analytical methods. The centre of mass of a body experiences two different types of accelerations namely,normal acceleration a^n and tangential acceleration a^t. Normal acceleration is a product of the angular velocity vector $\overrightarrow{\omega}$ and the linear velocity vector $\overrightarrow{\nu}$ where the latter can also be expressed as a vector product of the angular velocity $\overrightarrow{\omega}$ and displacement vector $\overrightarrow{r}$ as shown by

$$\begin{aligned} \overrightarrow{a^n} &= \overrightarrow{\omega} \times (\overrightarrow{\nu}) \\ \overrightarrow{\nu} &= \overrightarrow{\omega} \times \overrightarrow{r} \\ \overrightarrow{a^n} &= \overrightarrow{\omega} \times (\overrightarrow{\omega} \times \overrightarrow{r}) \end{aligned} \tag{3.32}$$

On the other hand, tangential acceleration is a cross product of angular acceleration vector $\overrightarrow{\alpha}$and the displacement vector $\overrightarrow{r}$ as given by

$$\overrightarrow{a^t} = \overrightarrow{\alpha} \times \overrightarrow{r} \tag{3.33}$$

Then the total acceleration a_{Total} is a summation of normal acceleration and tangential acceleration as in

$$\overrightarrow{a_{Total}} = \overrightarrow{a^n} + \overrightarrow{a^t} \tag{3.34}$$

The crank was assumed to rotate at uniform angular velocity and thus had zero angular acceleration and zero tangential acceleration. The acceleration for the centre of mass of the crank, G_2 was obtained by

$$
\begin{aligned}
\overrightarrow{a_{G2}} &= \overrightarrow{a^n} + \overrightarrow{a^t} \\
\overrightarrow{a^t} &= 0 \\
\overrightarrow{a_{G2}} &= \overrightarrow{a^n} \\
\overrightarrow{a_{G2}} &= \overrightarrow{\omega_2} \times (\overrightarrow{\omega_2} \times \overrightarrow{r_{AG2}}) \\
\overrightarrow{\omega_2} &= \omega_2 \hat{k} \\
\overrightarrow{r_{AG2}} &= \frac{b}{2}\{\cos\theta\hat{i} + \sin\theta\hat{j}\}
\end{aligned}
\tag{3.35}
$$

where $\overrightarrow{a_{G2}}$ is the linear acceleration vector for point $G2$, ω_2 was the angular velocity of the crank, $\hat{k}$ was a unit vector in the direction of rotation (z), and $\overrightarrow{r_{AG2}}$ was the displacement vector for point $G2$.

The acceleration vector for $G2$ was further split into its x and y components as given by

$$
\begin{aligned}
a_{G2_x} &= a_{G2}\cos\theta \\
a_{G2_y} &= a_{G2}\sin\theta
\end{aligned}
\tag{3.36}
$$

To get the acceleration of the centre of mass for the coupler ($G3$) the same procedure was followed. However, since its a floating link, the acceleration of crank-shared point B was first evaluated. This was done by considering point B as a point on the crank as shown

$$
\begin{aligned}
\overrightarrow{a_B} &= \overrightarrow{a^n} + \overrightarrow{a^t} \\
\overrightarrow{a^t} &= 0 \\
\overrightarrow{a_B} &= \overrightarrow{\omega_2} \times (\overrightarrow{\omega_2} \times \overrightarrow{r_{AB}}) \\
\overrightarrow{r_{AB}} &= a(\cos\theta\hat{i} + \sin\theta\hat{j})
\end{aligned}
\tag{3.37}
$$

where a_B is the linear acceleration of point B, ω_2 is the angular velocity of the crank, r_{AB} is the displacement vector of point B, and θ was the crank angl.

Then acceleration for point $G3$ was then obtained as

$$\begin{aligned}
\overrightarrow{a_{G3}} &= \overrightarrow{a_B} + \overrightarrow{a_{BG3}} \\
\overrightarrow{a_{BG3}} &= \overrightarrow{a^h} + \overrightarrow{a^t} \\
\overrightarrow{a_{G3}} &= \overrightarrow{a_B} + (\overrightarrow{\omega_3} \times (\overrightarrow{\omega_3} \times \overrightarrow{r_{BG3}})) + (\alpha_3 \times \overrightarrow{r_{BG3}})
\end{aligned} \tag{3.38}$$

where a_{G3} was the total acceleration of point $G3$, a_{BG3} was the acceleration of point $G3$ with respect to point B, ω_3 was the angular velocity of the coupler, r_{BG3} was the displacement vector of point $G3$ with respect to point B, and α_3 was the angular acceleration of the coupler.

Further definition of such vectors as ω_3, r_{BG3} and α_3 was required to fully compute the coupler centre acceleration.

$$\begin{aligned}
\overrightarrow{\omega_3} &= -\Big\{ \frac{a\omega_2 \sin(\varphi - \theta)}{b \sin(\varphi - \beta)} \Big\} \hat{k} \\
\overrightarrow{r_{BG3}} &= \overrightarrow{k_3}(\cos\beta \hat{i} + \sin\beta \hat{j}) \\
\overrightarrow{\alpha_3} &= \frac{1}{b \sin(\beta - \varphi)} \Big\{ -a\omega_2^2 \cos(\varphi - \theta) - b\omega_2^2 \cos(\varphi - \beta) \Big\}
\end{aligned} \tag{3.39}$$

The x and y components of the acceleration of the coupler centre were obtained as

$$\begin{aligned}
a_{G3_x} &= a_{G3} \cos\beta \\
a_{G3_y} &= a_{G3} \sin\beta
\end{aligned} \tag{3.40}$$

Finally, the acceleration for the centre of mass of the rocker ($G4$)was determined as

$$\begin{aligned}\overrightarrow{a_{G4}} &= \overrightarrow{a^n} + \overrightarrow{a^t} \\ \overrightarrow{a_{G4}} &= (\overrightarrow{\omega_4} \times (\overrightarrow{\omega_4} \times \overrightarrow{r_{G4D}})) + (\alpha_4 \times \overrightarrow{r_{G4D}})\end{aligned} \tag{3.41}$$

where ω_4 was the angular velocity of the rocker, $\overrightarrow{r_{G4D}}$ was the displacement vector of point $G4$, and α_4 was the angular acceleration of the rocker.

The angular velocity of the rocker,ω_4, was determined by (Doane, 2016)

$$\overrightarrow{\omega_4} = \Big\{ \frac{a\omega_2 \sin(\beta - \theta)}{c \sin(\beta - \varphi)} \Big\} \hat{k} \tag{3.42}$$

where ω_2 was the angular velocity of the crank, θ was the crank angle, φ was the rocker angle, $\hat{k}$ was the direction of rotation, a was the crank length, and c was the rocker length.

The displacement vector $\overrightarrow{r_{G4D}}$ was evaluated as

$$\overrightarrow{r_{G4D}} = \frac{c}{2}(\cos\varphi \hat{i} + \sin\varphi \hat{j}) \tag{3.43}$$

The angular acceleration, α_4, was obtained as follows (Doane, 2016)

$$\overrightarrow{\alpha_4} = \frac{1}{c \sin(\beta - \varphi)} \big\{ -a\omega_2^2 \cos(\beta - \theta) - b\omega_3 + c\omega_4 \cos(\beta - \varphi) \big\} \tag{3.44}$$

where b was the coupler length.

For the x and y components of the acceleration of the rocker centre, the following was done

$$\begin{aligned} a_{G4_x} &= a_{G4}\cos\varphi \\ a_{G4_y} &= a_{G4}\sin\varphi \end{aligned} \tag{3.45}$$

The nine equilibrium equations of the dynamic force analysis were then coded in MATLAB and used to calculate the unknown joint force values namely R_{12_x}, R_{12_y}, $R_{32_x}, R_{32_y}, R_{43_x}, R_{43_y}, R_{14_x}, R_{14_y}$, and T_3. The unknown torque T_3 was the output torque produced for every instance of the crank angle θ. The objective function for dynamic force, C_{DF} was given by

$$C_{DF} = \frac{1}{T_3} \tag{3.46}$$

The MATLAB code consisted of matrix M, which was a 9×9 matrix containing the coefficients of variables of the nine equilibrium equations. It also had a column vectors $\{X\}$ which carried the variables (internal forces and output torque) of the equilibrium equations which were to be evaluated. Another column vector $\{N\}$ contained the external forces, input torque and inertial forces found in each of the nine equations. The resultant system of equations was

$$M\{X\} = \{N\} \tag{3.47}$$

where M is a coefficient matrix, X is a variables matrix, and N is a known-forces matrix. Solving the system of equations gave the values of the unknowns. The code was as shown in Appendix C.

3.4 Effect of Link Lengths on the Motion and Force Transmission

The optimisation procedures discussed in this chapter aided in achieving particular optimal values of link lengths which gave optimum motion and force transmission. However, it would also be necessary to evaluate how change in the length of one link, while the others are held constant, affects the motion and transmission properties of the single-toggle jaw crusher model. This section is a sequel of the optimisation section carried before hand and borrows on the optimum length links obtained from optimisation when deciding on the link length values to be held constant. For instance, if the effect of crank length on the static force transmission is being sought after, the other links (coupler, rocker, and frame) are fixed at their optimum values as obtained from static force optimisation.

Notably, the effect cannot be evaluated for an undefined range of crank lengths. It must be sought for a range of crank lengths such that the entire four bar mechanism will operate smoothly, that is, the range of transmission angle, μ should be $40^0 \leq \mu \leq 140^0$. Therefore, the potential range is first determined before proceeding to explore how transition within such a range affects motion and force transmission.

Determining the potential range of link length requires two checks, one, checking the link length that gives the lowest smooth transmission angle, i.e. 40^0 and another evaluating the link length that achieves the highest smooth transmission angle, i.e. 140^0. The equation for the transmission angle of a four bar mechanism is given by

$$\cos\mu = \frac{b^2 + c^2 - a^2 - d^2 + 2adcos\theta}{2bc} \tag{3.48}$$

where μ is the transmission angle, a is the crank length, b is the coupler length, c is the

rocker length, d is the frame length, θ is the crank angle. From the proceeding, the lowest transmission angle is experienced when $\theta = 0^0$ while the highest transmission angle occurs when $\theta = 180^0$. The test for range of acceptable link lengths that can achieve the lowest transmission angle $\geq 40^0$ was carried out using

$$\cos 40^0 \geq \frac{b^2 + c^2 - e^2}{2bc} \tag{3.49}$$

where e is the diagonal in Figure 3.1.

On the other hand, the range of acceptable link lengths that can achieve the highest transmission angle $\leq 140^0$ was carried out using

$$\cos 40^0 \geq \frac{b^2 + c^2 - a^2 - d^2 + 2adcos\theta}{2bc} \tag{3.50}$$

.

3.5 Genetic Algorithm (GA)

Genetic Algorithm (GA) was chosen as the most preferred optimisation tool for this research courtesy of its superior information sharing strategy which assists in avoid local minima points. In addition, GA is best suited for functions which are non-differentiable and nonlinear as is the case with the objective functions in this chapter.

3.5.1 Genetic Algorithm (GA) Optimisation Code

The process required the definition of two functions: the objective function and the constraints function. The objective function first involved defining four variables to be optimised, representing the four linkages in the jaw crusher model. The time steps were also determined for the input shaft speed so that there were 360 time steps to

rhyme with the 360 deg of crank rotation. Typically, the speed of single toggle jaw crushers ranges from 200 rpm to 350 rpm (Donovan, 2003). Using the upper limit, the input shaft speed of 350 rpm (36 rad/s) was chosen for the position analysis. Position analysis followed for all joints in the model. Specifically, coordinates of the coupler-rocker joint were isolated and used to form the equation of the objective function.

3.5.2 Genetic Algorithm Constraints

Genetic algorithm requires constraint functions to guide the optimisation tool to search and obtain the best and practical link lengths required to optimise the objective function. Genetic algorithm constraints were classified into two types, namely, inequalities and equalities. The inequalities were in the form shown in equation 3.51.

$$Ax \leq b \tag{3.51}$$

where A is a matrix of variable coefficients and b is a vector of constants. Notably, the GA inequalities must be expressed in the form of less or equal to.

Meanwhile, the GA equality were in the form shown in equation 3.52.

$$A_{eq}x = b_{eq} \tag{3.52}$$

where A_{eq} is a matrix of variable coefficients and b_{eq} is a vector of constants.

Both GA equality and inequality constraints could be linear or nonlinear. In the current study, there were four constraints, all of them being inequalities. The inequalities were both linear and nonlinear where the latter must be defined within a

constrained function since equation 3.51 and 3.52 cannot capture nonlinearity. The four inequalities were:

1. For proper functioning of the crusher's four bar mechanism, the transmission angle was to be maintained between 40^0 and 140^0 (Balli & Chand, 2002). Transmission angle of a four bar mechanism is given by

$$\cos\mu = \frac{b^2 + c^2 - a^2 - d^2 + 2adcos\theta}{2bc} \tag{3.53}$$

   Inserting the values of transmission angle $\mu = 40^0$ and $\mu = 140^0$ and making the link lengths b, c, and d the subject of the equation, the following were obtained:

$$-2bc\cos(40) + b^2 + c^2 - (d-a)^2 \leq 0 \tag{3.54}$$

$$-b^2 - c^2 + 2bc\cos(140) + (d+a)^2 \leq 0 \tag{3.55}$$

2. No link was to be longer than the moving jaw (coupler). This was done since this link is the working link in the mechanism and thus the longer the better. Also, none of the links was to be shorter than the eccentricity (crank). This was in line with the requirements of a crank-rocker mechanism whereby the shortest link should be a side link and also an input link (Myszka, 2012). From this constraint, the set of expressions in Equation 3.56 was obtained. The first equation declared the crank to be shorter than the coupler while the second declared the frame to be longer than the crank. The third sought to ensure the rocker was shorter than the coupler while the fourth set the frame to be shorter than the coupler.

$$\begin{aligned} a - b &\leq 0 \\ a - d &\leq 0 \\ -b + c &\leq 0 \\ -b + d &\leq 0 \end{aligned} \tag{3.56}$$

3. The Grashof's condition (Ceccarelli, Ghosh, & Corves, 2015; Myszka, 2012) where for complete rotation of the crank, the sum of the lengths of the crank and coupler was to be smaller than the sum of the lengths of the other two links (frame and rocker). This condition is implemented in Equation 3.57

$$(a + b) - (c + d) \leq 0 \tag{3.57}$$

.

4. The range considered for the link lengths was between 10 mm and 600 mm. This range was chosen to correspond to the lengths of links in the preliminary design for this research where the longest link was 600 mm. The constraints were assembled into eight equations as shown in constraints code in Appendix D.

3.5.3 Optimisation Flowchart

The flowchart for the optimisation was shown in figure 3.11. Initial steps included the identification of variables to be optimised which , in this research, were the link lengths. This was followed by motion and force analysis which ultimately gave rise to the objective functions discussed in the various sections of this chapter. The steps that followed were carried out inside the MATLAB optimtool platform. Here, GA was chosen as the prefered solver and the number of variables defined as four. The

objective and constraints function were also passed to the solver and the lower and upper bounds established as 10 and 600 respectively. In addition, the solver options, namely initial population, crossover probability and mutation probability were set out as 200, 0.8 and 0.005 respectively as in the case of Zhao et al. (La-la et al., 2008). The stopping criteria was set at 10^{-6} function tolerance while the penalty factor was assigned as 10,000.

After the solver options were set, the solver was ran until the stopping criteria was met. The optimised results were then displayed.

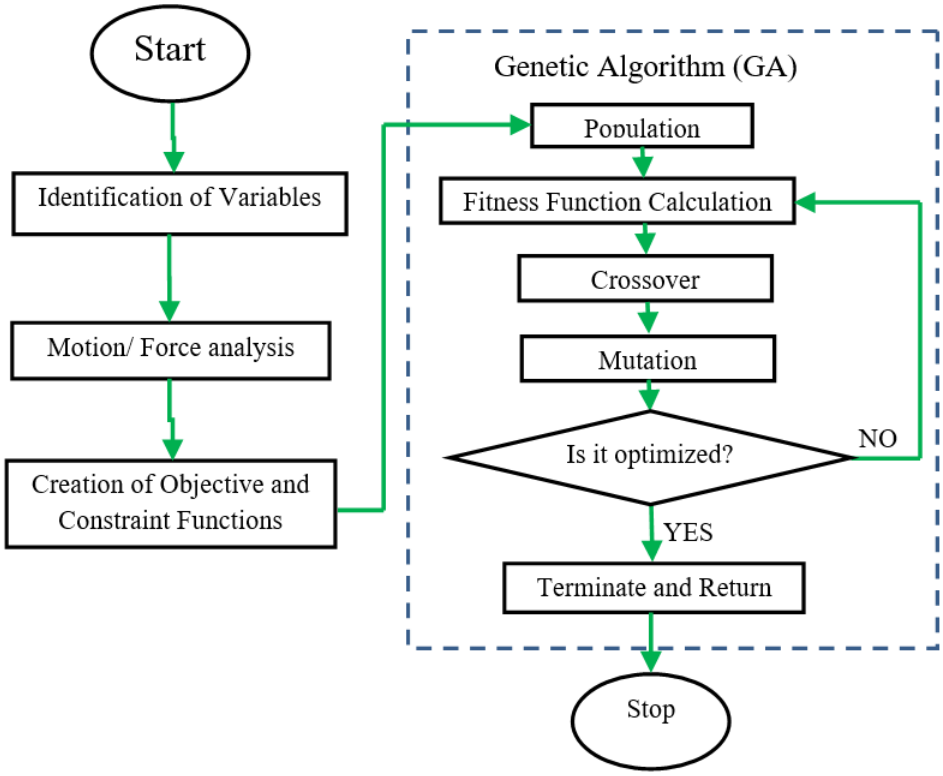

Figure 3.11: Flowchart for the development of the optimisation code

CHAPTER FOUR

RESULTS AND DISCUSSION

This chapter presents the results obtained from the GA optimisation of both motion and force objective functions. Under motion optimisation were two objective functions namely shearing-crushing ratio and crush travel inverse. For force optimisation, results are given for objective functions based on both static force and dynamic force analyses.

4.1 Motion Optimisation Results

There were two sets of motion optimisation results since two different objective functions were used. The two sets were as below:

4.1.1 Shearing-Crushing Ratio

4.1.1.1 Optimisation Results

When using the first objective function defined in Equation 3.7 which was based on both crushing travel and shearing travel, the GA process converged after four iterations giving the optimum value of the shearing-crushing ratio as well as the values of the four variables. The optimum values obtained were as follows:

1. The optimum value of the shearing-crushing ratio was 1.1816.
2. The optimum length of the crank, a, was 10 mm.
3. The optimum lengths of the coupler b, rocker (c), and the frame (d) were 600 mm.

From the above results, the lowest shearing-crushing ratio that could be obtained for a smooth functioning single-toggle jaw crusher four-bar model with the smallest link being the crank and the coupler being the longest was 1.1816. For every 1 mm moved in the crushing direction, the swing jaw experienced about 1.2 mm of shearing motion. These optimal results were obtained when the crank equalled the lower bound for the link lengths, that is, 10 mm and the other links were of length 600 mm.

The range of travel for different points on the swing jaw for the shearing-crushing optimised jaw crusher design was as shown in Figure 4.1.

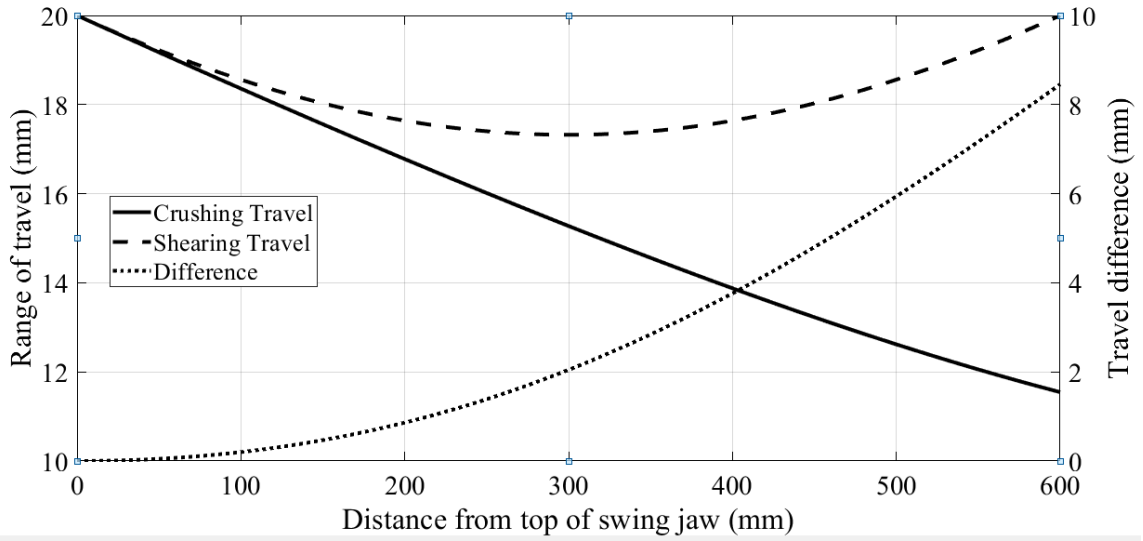

Figure 4.1: Travel Range for Swing Jaw of Shear-Crush Optimised Design

The shearing travel was parabolic with the vertex being at the middle of the swing jaw. Along the length, extreme jaw points had the greatest shearing displacements while the jaw centre had the lowest shearing displacement. Since the jaw load is applied to the fixed jaw, the profile of the latter should cater handle the different shearing scenarios. For instance, the fixed jaw plate centre would experience the least shear. The plate ends would have the greatest shear and were likely to wear out faster. The design of the plates for this jaw crusher mechanism should be concave

such that the greatest cross-sectional thickness is at the ends and the smallest at the centre as shown in Figure 4.2.

The crushing displacement decreased non-linearly from the top of the swing jaw to the bottom with a slightly decreasing gradient. This curve should spell the inclination of fixed jaw so that all parts of jaws have uniform loading as shown in Figure 4.2. The actual inclination was calculated as,

$$\delta = \sin\left\{\frac{C_R}{C_T}\right\} = \sin\left\{\frac{20 - 11.5452}{600 - 0}\right\} = 0.81^0$$

where, δ is the inclination angle of the fixed jaw, C_R is the crushing travel range, and C_T is the shearing travel range.

The difference between the shearing and crushing travels was non-linear increasing from zero at the swing jaw to maximum at the jaw bottom. Therefore, the point on the swing jaw with the biggest directional travel difference was the jaw bottom while the jaw top had the zero difference. The jaw top should be the strongest section of the jaw to deal with the high movements in both crushing and shearing directions. In addition, the big motion difference at the jaw bottom warrants the introduction of case-hardening materials such as low-carbon steel to help protect against excessive wear as shown in Figure 4.2

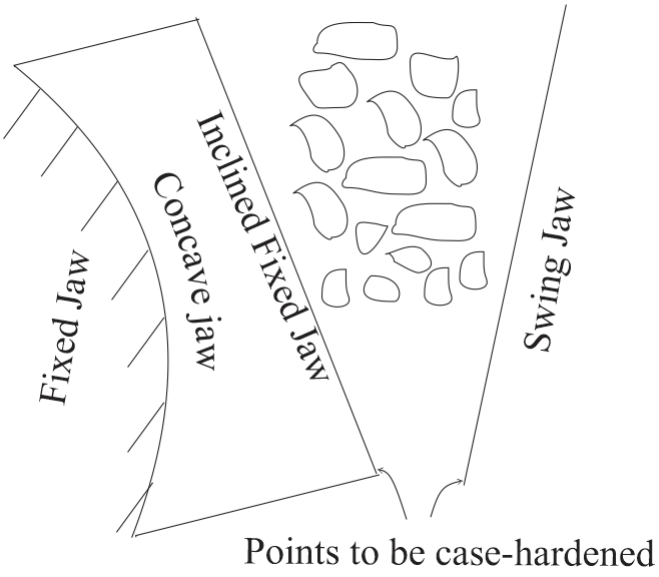

Figure 4.2: Shape of Fixed Jaw

Meanwhile, it would be adequate to consider the travel of the swing jaw bottom point when maximizing travel difference instead of considering the entire jaw. This would save on computational resources.

4.1.1.2 Effect of Link Lengths on the Shearing-Crushing Ratio

Before evaluating the effect of crank length on the characteristic travel, it was important to determine the range of crank length which obeyed Grashof's condition as shown in Equation 4.1.

$$a_{range} + b_{opt} \leq c_{opt} + d_{opt} \tag{4.1}$$

where a_{range} is the range of crank lengths, b_{opt} is the optimum coupler length, c_{opt} is the optimum rocker length, d_{opt} is the optimum frame length

From the above equation, the acceptable range of crank length was between 10 mm and 600 mm. Secondly, this range was evaluated for the transmission angle conditions

spelt out in Equation 3.49 and 3.50.

The range of crank lengths that could give a transmission angle $\geq 40^0$ was obtained by

$$\cos 40^0 \geq \frac{{b_{opt}}^2 + {c_{opt}}^2 - ({a_{range}}^2 + {d_{opt}}^2 - 2 \times a_{range} \times d_{opt})}{2 \times b_{opt} c_{opt}} \tag{4.2}$$

as 10 mm $\leq a_{range} \leq$ 189 mm. Crank lengths above 189 mm gave transmission angles lower than 40^0 which is undesirable.

Meanwhile, the range of crank lengths that could give a transmission angle $\leq 140^0$ was achieved by

$$\cos 140^0 \leq \frac{{b_{opt}}^2 + {c_{opt}}^2 - ({a_{range}}^2 + {d_{opt}}^2 + 2 \times a_{range} \times d_{opt})}{2 \times b_{opt} c_{opt}} \tag{4.3}$$

as $a_{range} \leq 527$ mm meaning all link lengths below this value could give transmission angles less than 140^0.

Combining the two ranges of crank lengths, the effective length for the crank for smooth transmission was between 10 mm and 189 mm. With the crank range already determined, its effect on the crushing-shearing ratio was investigated as shown in Figure 4.3.

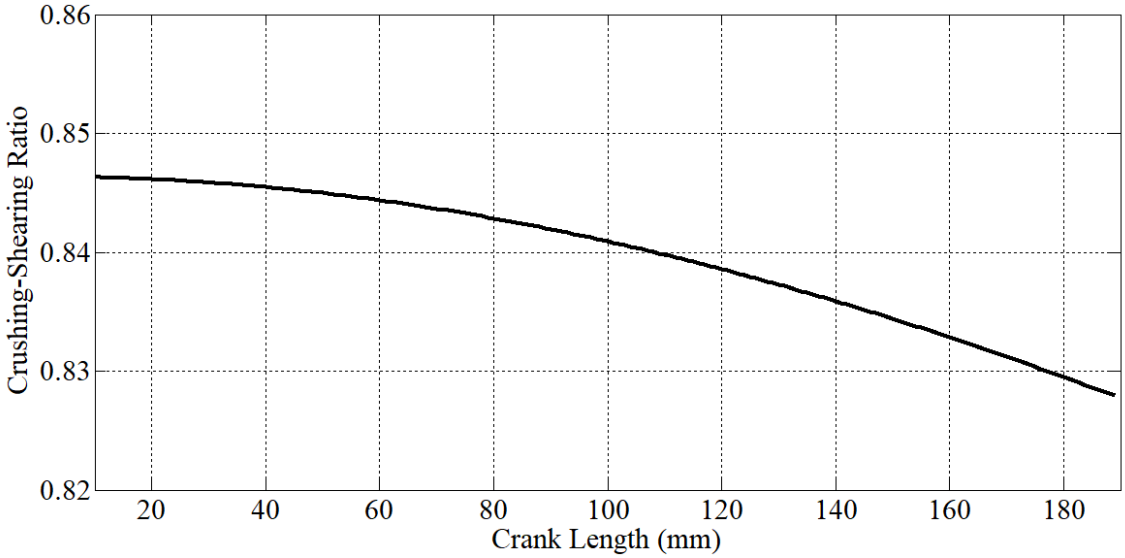

Figure 4.3: Crushing-shearing ratio vs crank length

The relationship between the crank and the crushing-shearing ratio was nonlinear. The ratio declined with increase in crank length showing the superiority of shorter eccentricity in jaw crusher performance. At the lowest crank size, that is, 10 mm, the crusher would experience the combination of highest crushing capacity via improved travel in the crushing direction as well as least wear problems by reducing the shearing travel. The input forces at the eccentric shaft would most efficiently be converted to useful crushing work thus reducing energy wastage in form of wear and heat which occur due to shearing.

The effect of other links on the crushing-shearing ratio was also evaluated. To get the coupler length limits allowable for smooth operation of the jaw crusher mechanism at 0^0 crank angle , the following was done,

$$\cos 40^0 \geq \frac{{b_{range}}^2 + {c_{opt}}^2 - ({a_{opt}}^2 + {d_{opt}}^2 - 2 \times a_{opt} \times d_{opt})}{2 \times b_{range} c_{opt}} \tag{4.4}$$

where, b_{range} is the range of coupler lengths. The coupler range for minimum

transmission angle was $13.13 \leq b_{range}$. The coupler range for maximum transmission angle was given by

$$\cos 140^0 \leq \frac{{b_{range}}^2 + {c_{opt}}^2 - ({a_{opt}}^2 + {d_{opt}}^2 + 2 \times a_{opt} \times d_{opt})}{2 \times b_{range} c_{opt}} \tag{4.5}$$

as $b_{range} \leq 12.98$. From Equations 4.4 and 4.5, the allowable range for coupler length was $13.13 \leq b_{range} \leq 600$ mm. The influence of the coupler length range was as shown in Figure 4.4. The figure shows two different sections of coupler influence. The initial section between $14 - 109$ mm indicated a sharp nonlinear increase in the crushing-shearing ratio. This could be explained by the maximum transmission angle being at 90^0 and the minimum transmission angle being highest (closest to 90^0) as shown in figure 4.5.

The transmission angles approaching the 90^0 mark so that the crushing component corresponding to sine of the transmission angle increased and the shearing component corresponding to the cosine of the angle decreased; the result was an increase in the crushing-shearing ratio.

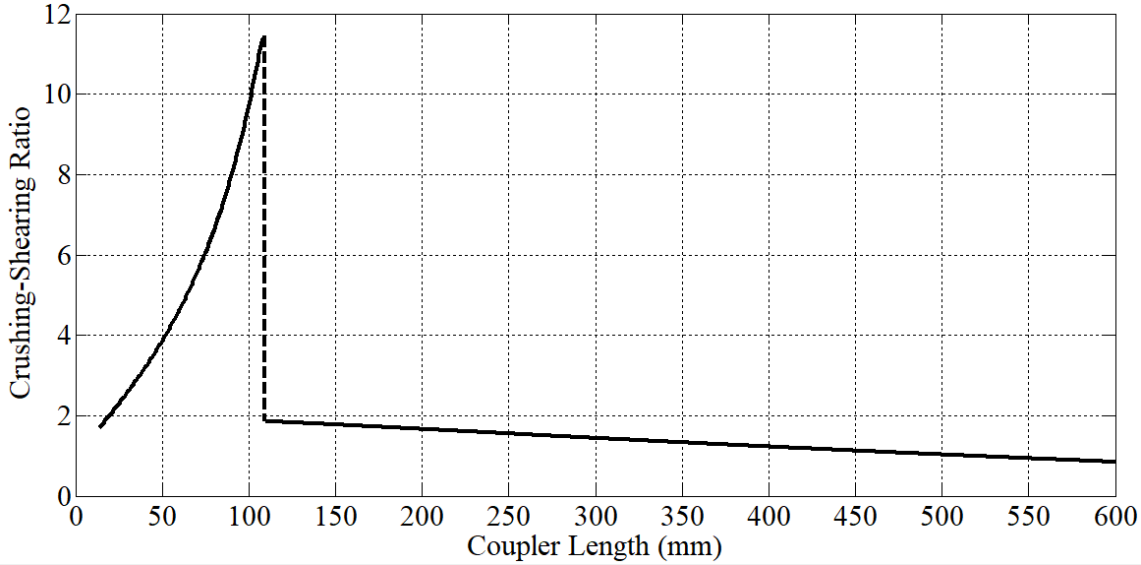

Figure 4.4: Crushing-shearing ratio vs coupler length

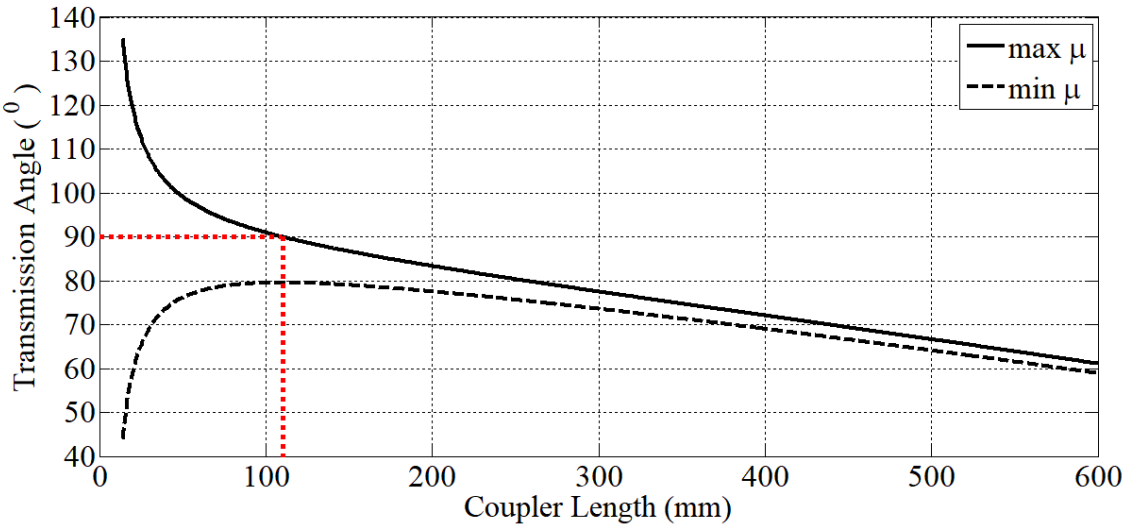

Figure 4.5: Transmission angle vs coupler length

A discontinuity occured at 110 mm coupler length. The discontinuity represented a mechanism which had an instance of 90^0 transmission angle in which case the shearing motion was dominant and according to Equation 3.7, the ratio dropped rapidly. Between $110 - 600$ mm, the ratio decreased gradually in a linear trend. Within this range, both the maximum and minimum transmission angles dropped further away from 90^0 towards 0^0 as shown in figure 4.5. Thus the crushing area values (sine related) decreased while the shearing values (cosine related) increased causing the ratio to drop.

From figure 4.4, 109 mm was found to be the most suitable length of the swing jaw for the highest crushing-shearing ratio. At this length, the swing jaw would maximise crushing travel and minimise shearing motion thus saving on energy wastage as well as reducing jaw plate wear. Therefore, instead of using a 600 mm coupler length, one of 109 mm would suffice and still perform effective crushing as well as reduce jaw plate wear. This would help in material conservation and reduction in production costs.

The range used for the coupler could also be applied for the rocker because of their

similar positioning in the transmission angle Equation 3.48 and similar optimum values. Figure 4.6 shows the relationship between the rocker length and the crushing-shearing ratio while maintaining other links at their optimum length values.

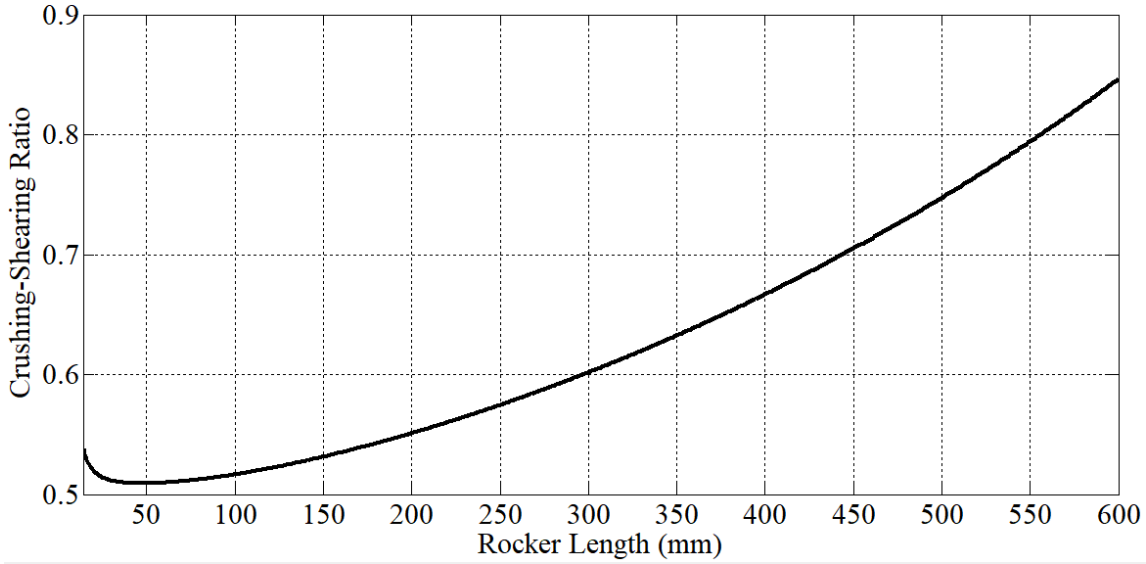

Figure 4.6: Crushing-shearing ratio vs rocker length

From Figure 4.6, the crushing-shearing ratio decreased steeply between 14 mm and 48 mm. It then increased almost linearly between 48 mm and 600 mm. The minimum value was 0.5 at 48 mm while the highest value was 0.85 at 600 mm. Subsequently, a mechanism with a toggle plate of 600 mm would have the highest crushing capacity with the least shear-related wear problems. Initially, the transmission angles approached 90^0 increasing motion transmission to the rocker as well as shear motion in the coupler. From 48 mm, the transmission angles decreased from 90^0 decreasing shear motion in coupler but increasing crushing motion and thus the rise in the crushing-shearing ratio.

For the frame, the length limits were determined from Equation 4.6 and 4.7.

$$\cos 40^0 \geq \frac{{b_{opt}}^2 + {c_{opt}}^2 - ({a_{opt}}^2 + {d_{range}}^2 - 2 \times a_{opt} \times d_{range})}{2 \times b_{opt} c_{opt}} \tag{4.6}$$

where d_{range} was the range of coupler lengths and the resultant suitable range that gave minimum transmission angle $\geq 40^0$ was $d_{range} \geq 420.46$ mm. Equation 4.7 was used for proper functionality of the mechanism at crank angle 180^0.

$$\cos 140^0 \leq \frac{{b_{opt}}^2 + {c_{opt}}^2 - ({a_{opt}}^2 + {d_{range}}^2 + 2 \times a_{opt} \times d_{range})}{2 \times b_{opt} c_{opt}} \tag{4.7}$$

The most suitable range for maximum transmission angle requirements was $d_{range} \leq$ 1,117. This was beyond the maximum set link length of 600 mm and thus the latter was chosen as the upper limit of the range so that the frame length range was $420.26 \leq d_{range} \leq 600$ mm. The effect of the frame length was graphed within these limits as shown in Figure 4.7.

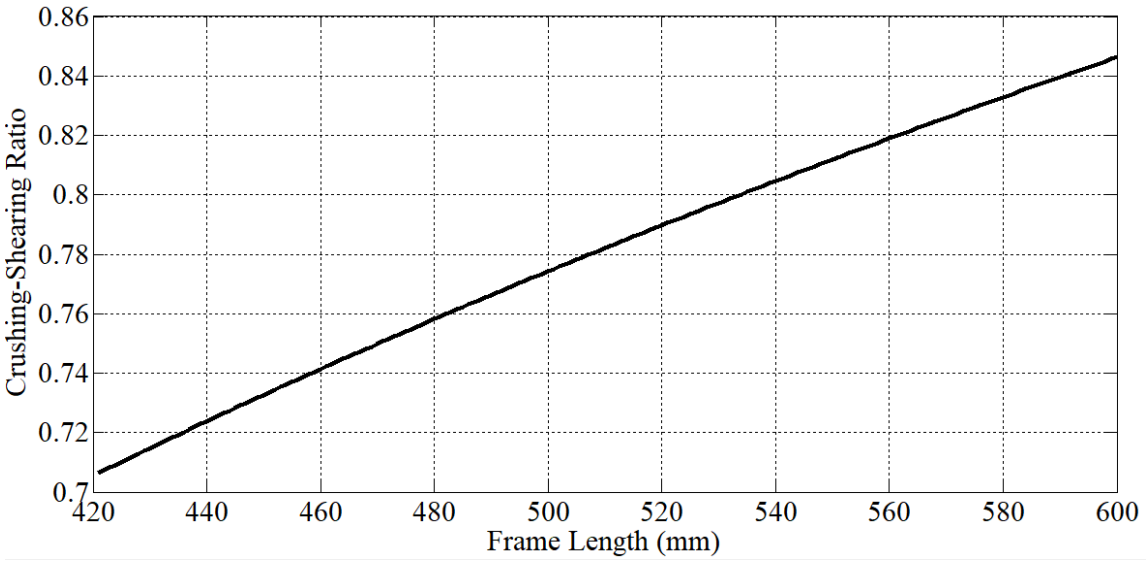

Figure 4.7: Crushing-Shearing Ratio vs Frame Length

The relationship between the frame and the crushing-shearing ratio was almost linear with a positive gradient between 421 mm and 600 mm. A ground link of 600 mm would be the best for optimum crushing potential of the single-toggle jaw crusher.

4.1.2 Crush Travel Inverse

4.1.2.1 Optimisation Results

The second characteristic travel was based on crushing travel only and was defined as per Equation 3.8. The function converged after four iterations and the following results were obtained:

1. The optimum value of the crush travel inverse was 5.7818×10^{-6} mm^{-2}.
2. The optimum length of the crank, a was 189 mm.
3. The optimum lengths of the coupler (b), rocker(c) and the frame (d) was 600 mm.

The mechanism optimised for maximum crushing travel achieved a total travel area of 172,956.52 mm^2 for all points on the crushing jaw. Assuming a unit width of 1 m for the crusher, the capacity produced by the optimised design in one crank revolution was 1.7296 $\times 10^{-4} m^3$. This translated to 3.5676 m^3/hr and 28.54 m^3/day for an 8-hour day shift. This amount could fill a 10 tonne tipper truck.

Compared to the shearing-crushing ratio, the link lengths for the crush travel optimised mechanism were similar except for the crank whose length in this case was 189 mm. The crank made the difference between the two travel characteristics cases. In the first case, the optimum value of the mechanism occured when the crank length was at its lowest, that is, 10 mm. In the second characteristic, the best mechanism had the crank length being at its highest, that is, 189 mm.

The range of travels for different points on the swing jaw for the optimised jaw crusher design under the crush travel inverse were as shown in Figure 4.8.

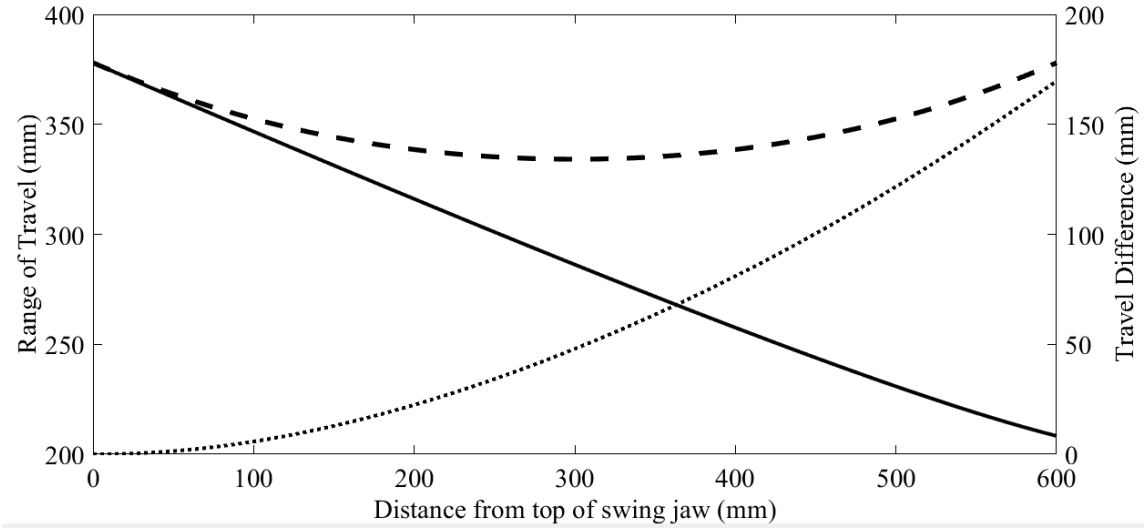

Figure 4.8: Travel Range for Swing Jaw Points of Crush Optimised Design

The travel properties of the crush-travel-inverse optimised design were replica to the shearing-crushing ratio optimised design but varied in magnitude. The former had almost 200% more travel than the latter in both shearing and crushing directions. For instance, a crush-optimised mechanism achieved a crushing travel of 380 mm while a crushing-shearing-ratio optimised crusher could only manage 20 mm as shown in Figure 4.1. The same was observed for the difference in travel.

4.1.2.2 Effect of Link Lengths on the Crush Travel Inverse

Similar to the shearing-crushing ratio case, the effect of each of the link lengths was also done for the crush travel inverse case. Figure 4.9 shows the effect of crank length.

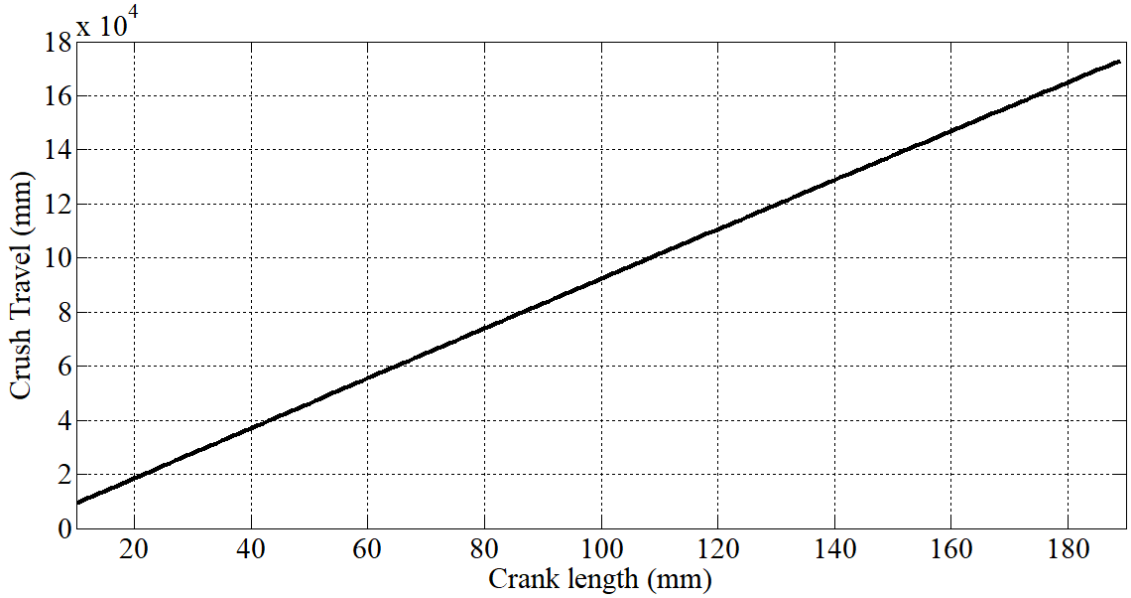

Figure 4.9: Crush Travel vs Crank Length

In the figure, there is a linear relationship between the crank length and the crushing travel. Increasing the eccentricity of the jaw crusher would improve its crushing capacity linearly.

The length of the coupler affected the second characteristic travel as shown in Figure 4.10

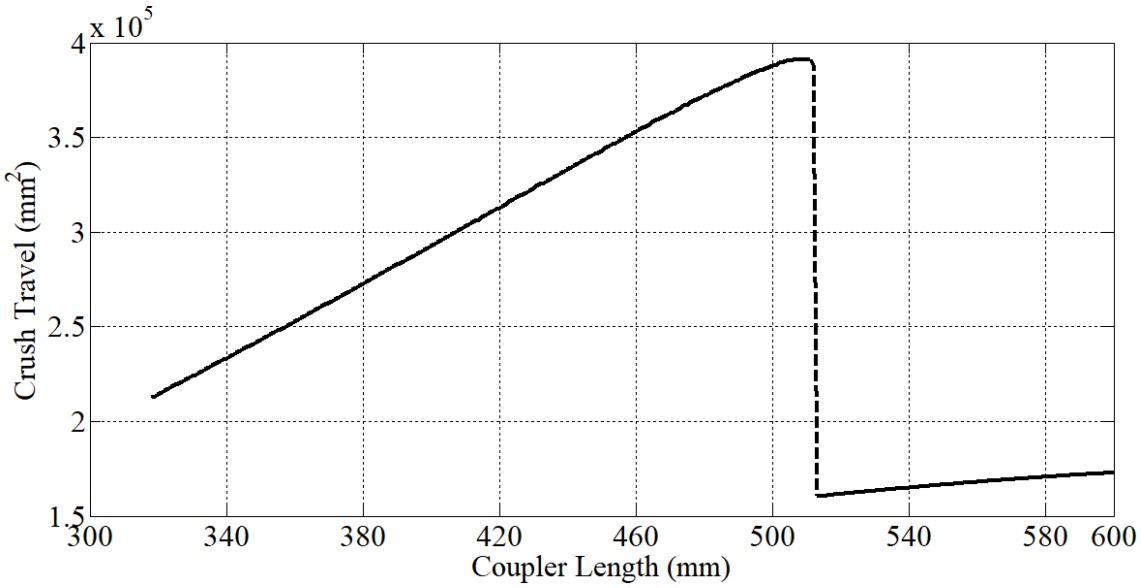

Figure 4.10: Crush Travel vs Coupler Length

The figure shows that the influence of coupler length had two sections. Initially, the crush travel increased almost linearly with increase in the coupler length from 318 mm to 511 mm. In this section, the maximum transmission angle decreased from obtuse towards 90^0. The crushing travel also increased since it is directly related to the sine of the transmission angle.

A discontinuity occured between length 512 mm and 513 mm. The discontinuity marked the point where the transmission angle reached 90^0. At that length, the coupler was only moving in the shearing direction and had no crushing component. This section was of interest since the best crushing would happen just before it, at length 511 mm.

Finally, the second section involved a linear relationship between the crush travel and the coupler length for the range $513 - 600$ mm. In this section, the crush travel improved slightly with increase in coupler length. This section showed minimal increase in crushing travel. The coupler design would save on material by reducing its length from 600 to 511 mm without reducing crushing efficiency.

The effect of the rocker length on the crush travel was also done as per Figure 4.11.

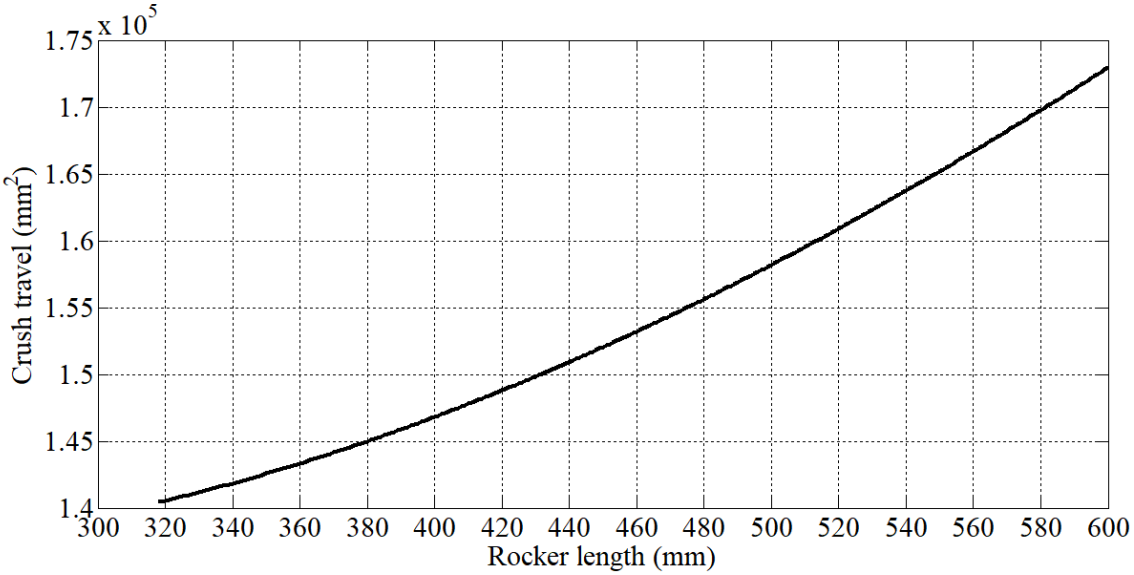

Figure 4.11: Crush Travel vs Rocker Length

Figure 4.11 showed a positively sloped almost linear relationship between the crush travel and the rocker length. Longer toggle plates would give better crushing capacity and vice versa. The best length would be 600 mm and the least desirable at 318 mm.

The frame was different. When the other link lengths were taken as constants at their optimum values, the allowable frame length range was found as per Equation 4.8 and 4.9 to check proper functionality at crank 0^0 and 180^0 respectively.

$$\cos 40^0 \geq \frac{{b_{opt}}^2 + {c_{opt}}^2 - ({a_{opt}}^2 + {d_{range}}^2 - 2 \times a_{opt} \times d_{range})}{2 \times b_{opt} c_{opt}} \tag{4.8}$$

where d_{range} was the range of coupler lengths and the resultant suitable range that gave minimum transmission angle $\geq 40^0$ was $d_{range} \geq 420.46$ mm. Equation 4.9 was used for proper functionality of the mechanism at crank angle 180^0.

$$\cos 140^0 \leq \frac{{b_{opt}}^2 + {c_{opt}}^2 - ({a_{opt}}^2 + {d_{range}}^2 + 2 \times a_{opt} \times d_{range})}{2 \times b_{opt} c_{opt}} \tag{4.9}$$

From both equations, the allowable frame length range was $d \geq 599.4$. Therefore, if all links were to be less than 600 mm, the influence of the frame could not be graphed since it would only show a single point. Noticeably, due to the high value of optimum crank length, the range of frame length diminished.

4.2 Force Optimisation

Force optimisation results obtained were as discussed in the sections below.

4.2.1 Static Force Optimisation

4.2.1.1 Optimisation Results

Optimisation of the static force in a single-toggle jaw crusher mechanism model was done using the objective function in equation 3.20. The results obtained were as follows:

1. The optimum value of the objective function was 2.3502e-09 $(\text{Nm})^{-1}$.
2. The optimum length of the crank, (a) was 214 mm.
3. The optimum length of the coupler (b) was 600 mm.
4. The optimum length of the rocker (c) was 443.78 mm.
5. The optimum lengths of the frame (d) was 600 mm.

The variation of static torque with crank angle was evaluated for the above optimised mechanism as shown in Figure 4.12.

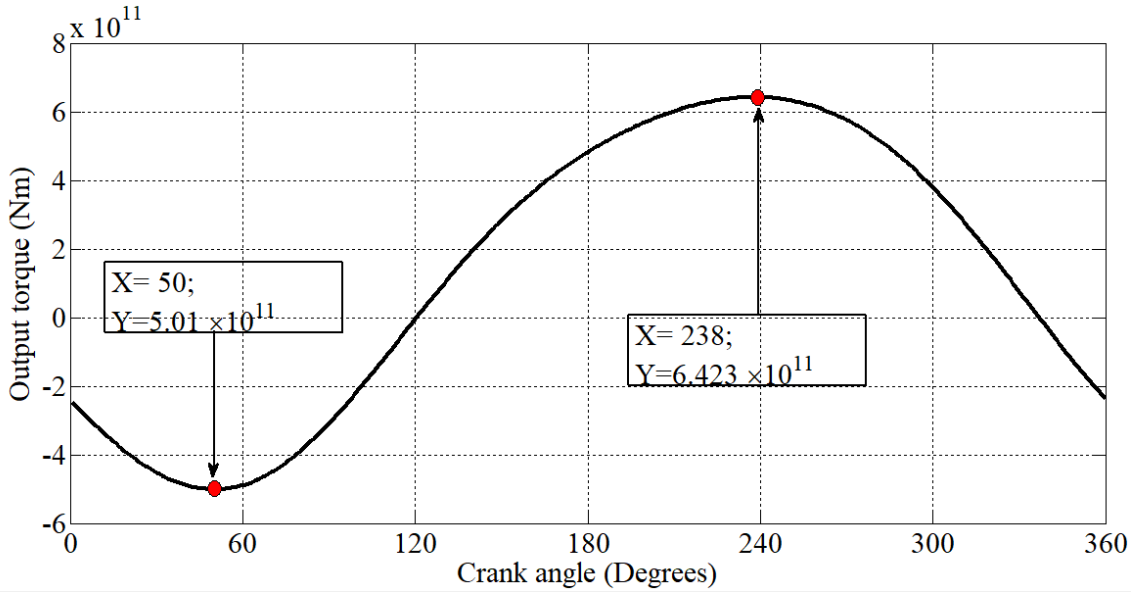

Figure 4.12: Static torque of the coupler-rocker joint against crank angle

The crushing stroke for the mechanism was between 122^0 and 337^0 while the idle stroke had two portions: $0^0 - 121^0$ and $338^0 - 360^0$. The total angle for the crushing stroke was 216^0, leaving 144^0 for retraction in the idle stroke. Consequently, the mechanism had quick return properties with a time ratio of 1.5 between the working stroke and return stroke. From the input torque, this jaw crusher would experience 1.5 times as much rock crushing torque as jaw retraction torque. A higher time ratio is thus desirable for the single-toggle jaw crusher as it directly benefits crushing efficiency.

The highest output torque during crushing was $6.4232\text{e}{\times}10^{11}$ Nm at crank angle 238^0 which was approximately midway into the stroke. Most rocks would be crushed halfway into the crushing stroke where the output torque is maximum. During the swing jaw retraction, the highest torque was -5.010×10^{11} Nm at 50^0 crank angle. This maximum value was also almost midway into the idle stroke as was in the crushing case. Therefore, most static torque in the jaw crusher is required midway through the respective strokes (crushing and idle strokes) thus the midway torque

could be assumed as the design output torque for the input eccentric shaft.

4.2.1.2 Effect of Link Lengths on Static Torque

After realising the design with optimised force transmission, it was also necessary to understand the effect each link length on the output crushing torque. This was done while also considering the Grashof's condition and transmission angle constraints. Figure 4.13 shows the influence of the crank length on the crushing torque.

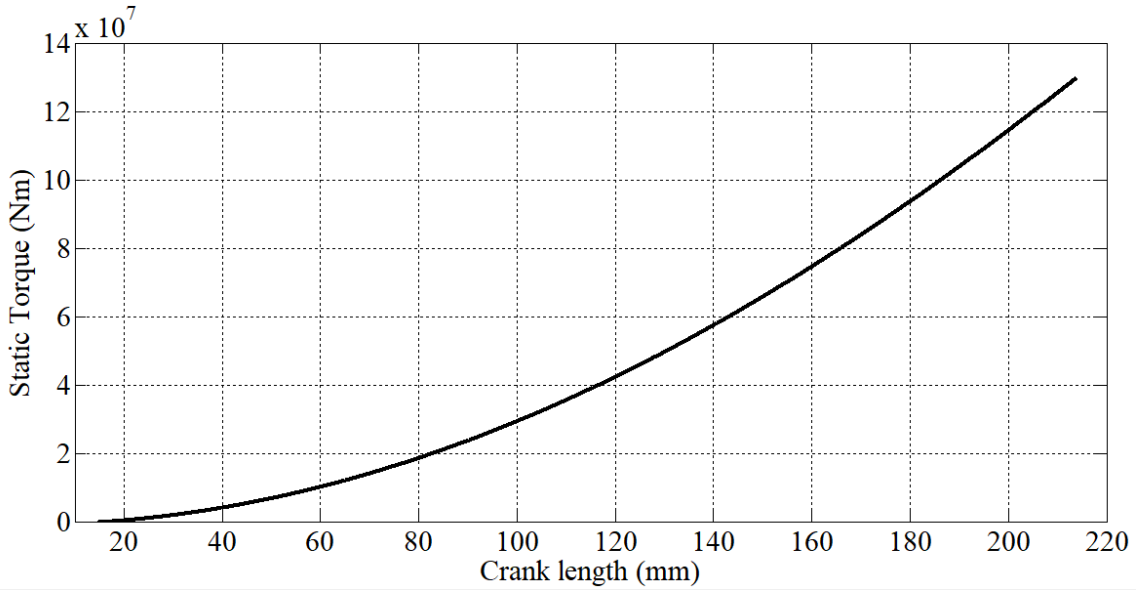

Figure 4.13: Output Crushing Torque vs Crank Length

There was a parabolic relationship between static torque and crank length. An increase in the crank length would lead to better high static torque being produced at the swing jaw for better comminution.

The crushing torque was affected by the coupler length as shown in Figure 4.14.

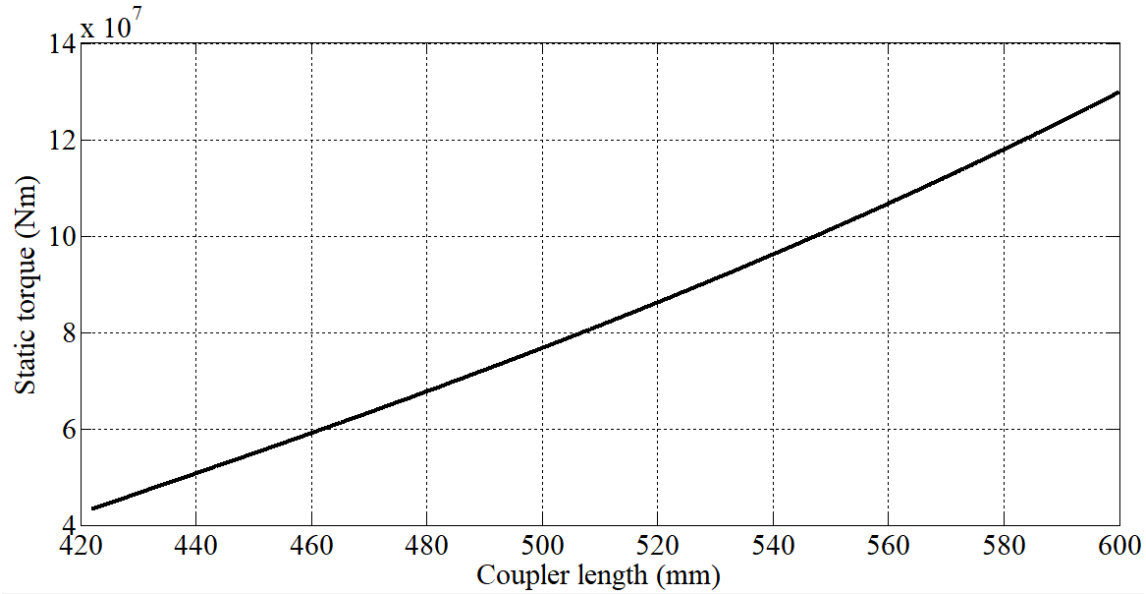

Figure 4.14: Output Crushing Torque vs Coupler Length

The figure showed a slightly nonlinear relationship between the coupler and static torque. Generally, longer swing jaws would provide more torque compared to shorter ones. It is desirable to increase the length of the swing jaw to obtain the most crushing capacity for the single toggle jaw crusher. A coupler of 600 mm will give greater production compared to one of 430 mm though at the expense of material cost.

The rocker length considered was between 443.78 mm and 475.47 mm. The effect of rocker length variation on the output torque was as shown in Figure 4.15.

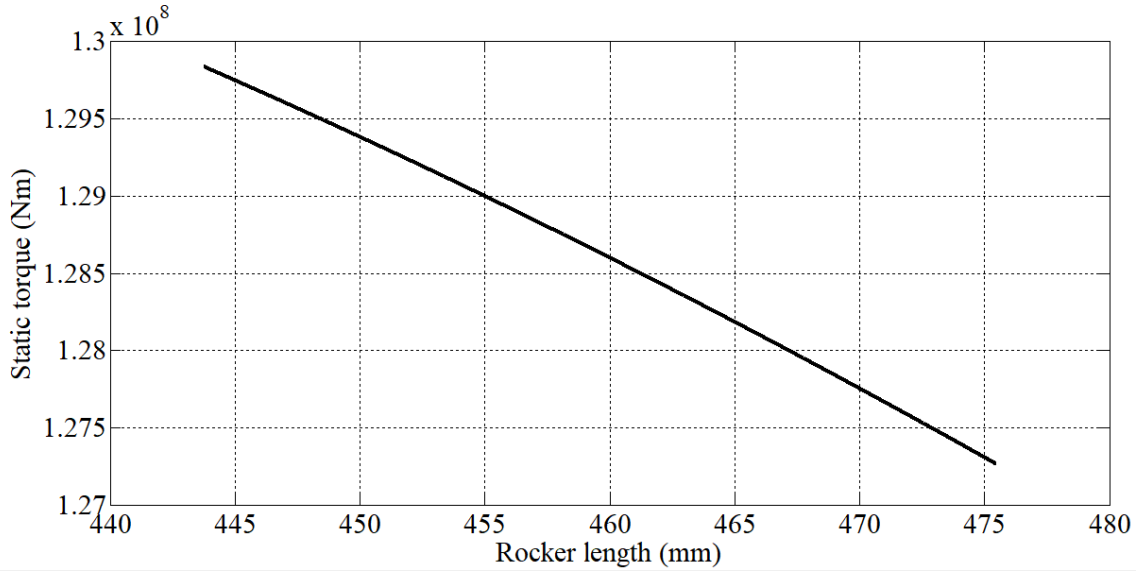

Figure 4.15: Output Crushing Torque vs Rocker Length

Figure 4.15 shows a non-linear effect of rocker length on static torque. Static torque decreased with increase in rocker length for the range considered. The highest torque was obtained at 443.78 mm. A toggle plate of this length would produce the greatest crushing torque and thus the best productivity for a single toggle jaw crusher. Since the shortest rocker length gave the highest torque, this would help in material saving and thus material cost reduction.

As for the frame length, its effect on the crushing torque could not be determined since only the optimum length, 600 mm satisfied the transmission angle conditions. Lengths below this value gave transmission angles below 40^0 which would result in jamming of the mechanism.

Using the 40^0 transmission angle condition, the frame length range was determined using

$$\cos 40^0 \geq \frac{{b_{opt}}^2 + {c_{opt}}^2 - ({a_{opt}}^2 + {d_{range}}^2 - 2 \times a_{opt} \times d_{range})}{2 \times b_{opt} c_{opt}} \tag{4.10}$$

as $d \geq 600$. Meanwhile, the upper transmission angle limit condition was used in

$$\cos 140^0 \leq \frac{{b_{opt}}^2 + {c_{opt}}^2 - ({a_{opt}}^2 + {d_{range}}^2 + 2 \times a_{opt} \times d_{range})}{2 \times b_{opt} c_{opt}} \tag{4.11}$$

to give a range of $d \leq 768$. Consequently, the acceptable range of frame was between 600 mm and 768 mm which was beyond the limit considered in this research thus no frame effect plot could be made.

4.2.2 Dynamic Force Optimisation

4.2.2.1 Optimisation Results

Optimisation of the dynamic force in a single-toggle jaw crusher mechanism model was done using the objective function in equation 3.46 . The results obtained were as follows:

1. The optimum value of the objective function was $1.5625 \times 10^{-12}(Nm)^{-1}$
2. The optimum length of the crank, *(a)* was 10.26 mm.
3. The optimum length of the coupler (b) was 600 mm.
4. The optimum length of the rocker (c) was 500 mm.
5. The optimum lengths of the frame (d) was 552.5 mm.

The spread of the output torque over the crank revolution was as shown in Figure 4.16 while the graph of angular acceleration is plotted figure 4.17 for comparison.

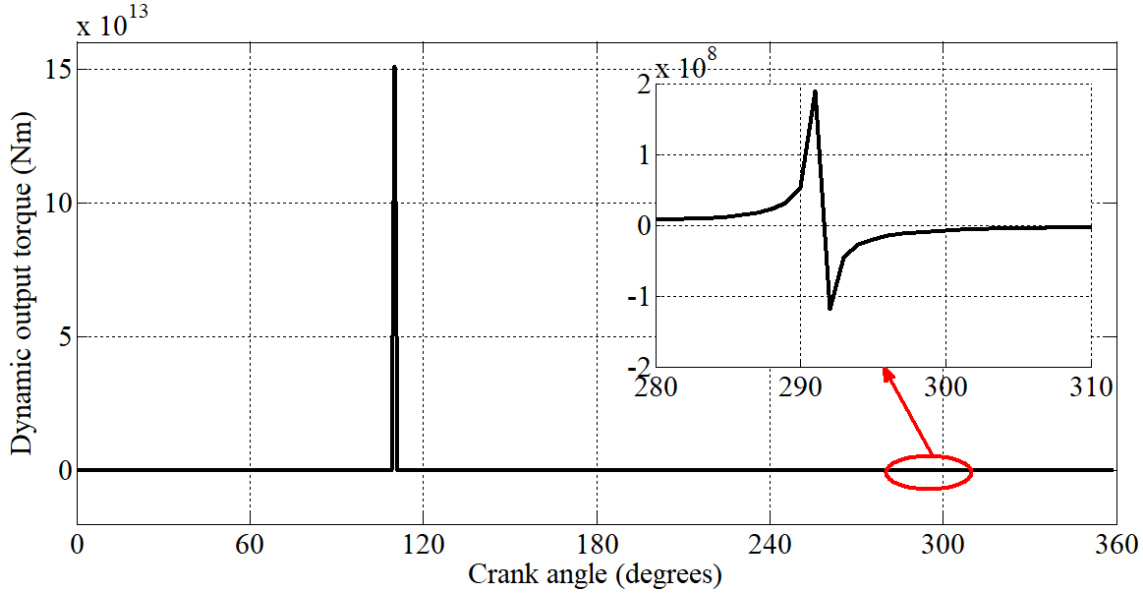

Figure 4.16: Output Torque vs Crank Angle

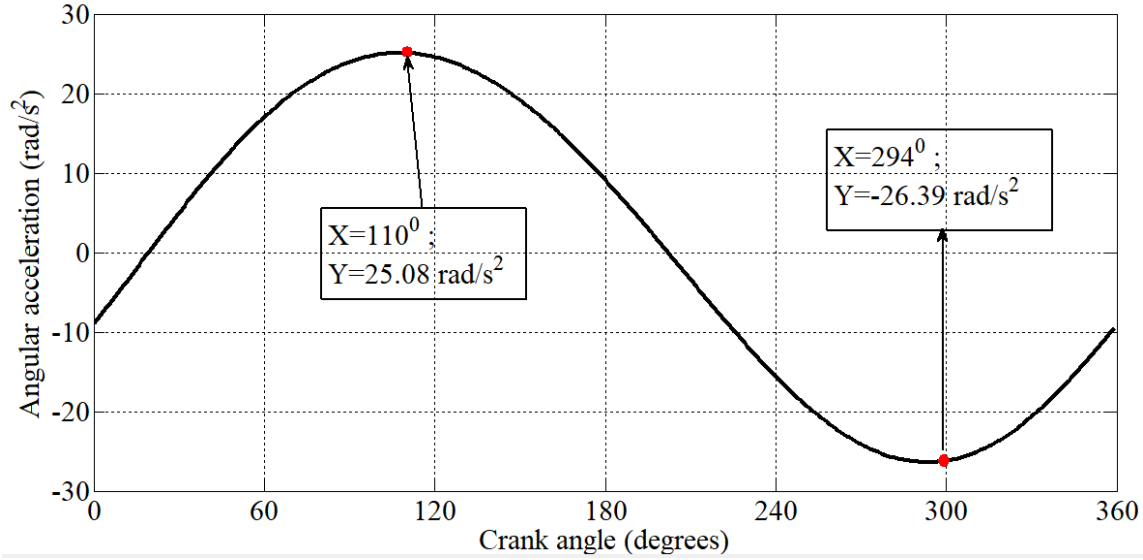

Figure 4.17: Points of Maximum and Minimum Angular acceleration

The maximum torque was obtained at 110^0 crank angle as shown in Figure 4.16. Most of the rock crushing would occur at this crank angle. This maxima coincided with the point of maximum angular acceleration of the swing jaw as shown in Figure 4.17 because torque and angular acceleration are directly proportional properties.

A second peak of lower magnitude existed at 294^0 as shown in the break out plot in Figure 4.16. It coincided with the minimum acceleration of the swing jaw as per Figure 4.17. The jaw crusher would also have considerably high crushing capacity at this angle. The difference between the first and second peaks could be explained by transmission angles at the two crank angles. At the high peak, the transmission angle was higher and thus more torque obtained from the mechanism compared to the second peak.

Notably, the two crank angles, 110^0 and 294^0 marked the end of their respective crushing strokes. Peak torques occured at the transition from crushing to retraction stroke. It can then be concluded that during a crushing stroke, most of the crushing would occur at the end of the stroke when the jaw crusher is nearest to the fixed jaw. Feeding should be done such that it is approximately when the jaws are closing to avoid clogging and for best crushing results.

The crushing stroke occured from 0^0 to 110^0 as the swing jaw approached the fixed jaw. At 110^0, the swing jaw had maximum acceleration as it came closest to the fixed jaw and its angular velocity dropped to zero. The same observation was made at 294^0, still at the end of another crushing stroke. These were limiting positions of the jaw crusher mechanism and massive torques were required to drive the mechanism out of them. This explains the high instantaneous torques observed at the the two points.

According to Figure 4.16, the crushing stroke covered 236^0 of crank rotation which acccounted for almost 66% of the entire cycle of motion. The mechanism had a time ratio of 1.90 meaning it was a significantly superior quick return mechanism. This feature meant 66% of the motor torque at the eccentric shaft was converted to useful rock crushing energy at the swing jaw while the remainder was used for retraction.

4.2.2.2 Effect of Link Lengths on Dynamic Torque

As opposed to the other responses considered so far which were either linear or non-linear, the effect of link lengths on the dynamic torque response had a non-periodic trend characterised by peaks which occured at certain link lengths. The peak lengths were crucial as they represented link lengths at which high dynamic torque could be obtained and consequently high transmission forces for effective crushing. In each case, the peaks were highlighted as shown in Figure 4.18, 4.19, 4.20, and 4.21. The variation of dynamic torque with crank length was as shown in Figure 4.18.

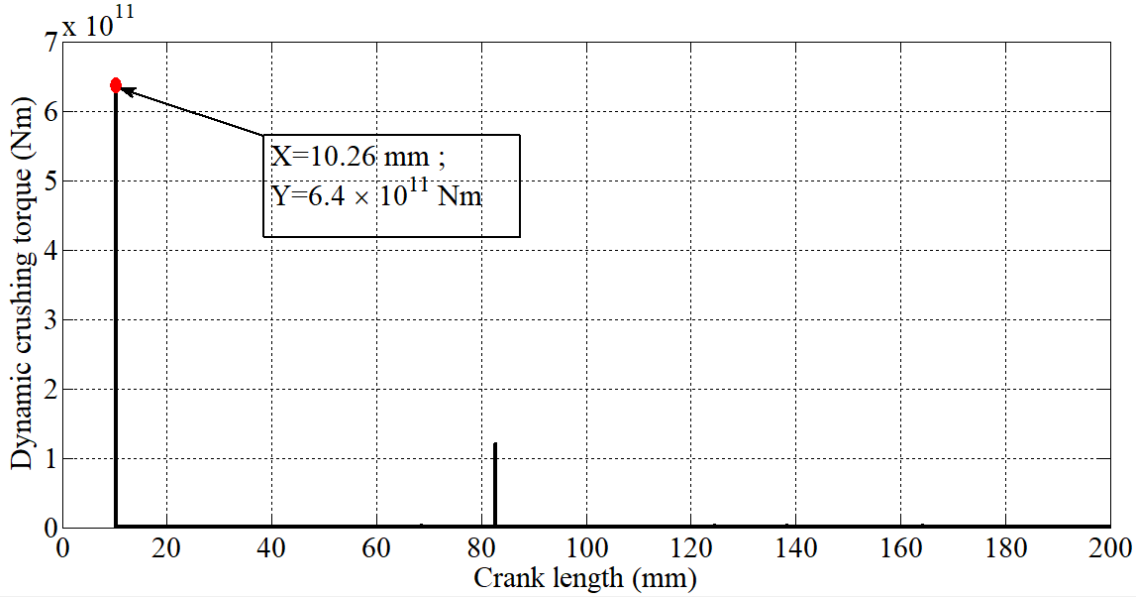

Figure 4.18: Dynamic Crushing Torque vs Crank Length

The highest dynamic torque was achieved at crank length 10.26 mm. There was another significant peak at 82.76 mm but of lower magnitude at 1.212×10^{11} Nm. A jaw crusher with an eccentricity of 10.26 mm would have 6.4002×10^{11} Nm crushing torque with all other lengths kept constant at their optimum values. This length would give the greatest stone production due to the high output torque. The 10.26 mm crank length also represented a huge saving on link material without neglecting

torque transmission and crusher capacity.

Next, the influence of change in the coupler length was as shown in Figure 4.19.

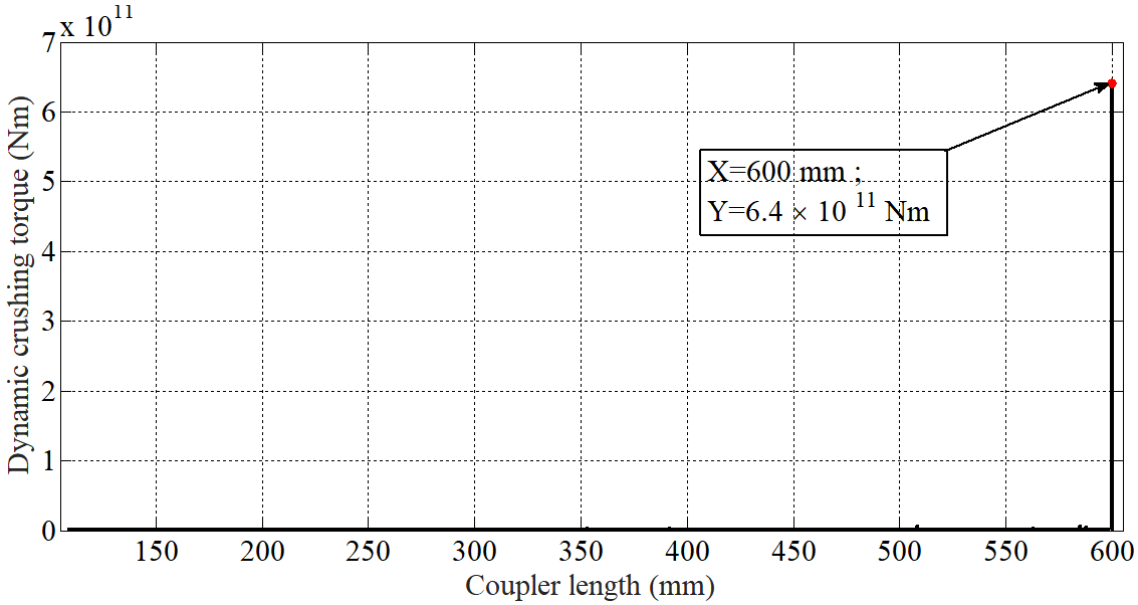

Figure 4.19: Dynamic Crushing Torque vs Coupler Length

One peak was prominent in Figure 4.19. Its value was 6.4002×10^{11} Nm and occured at coupler length 600 mm. Notably, 600 mm was the upper limit of the range considered. Similar observations were made for other responses such as the shearing-crushing ratio, crush travel inverse and static torque. It can be concluded that the coupler should be the longest link in the jaw crusher model and should match with the maximum length allowable for higher crusher production. The long coupler length also served to enhance crusher capacity by increasing the length of swing jaw in contact with the rocks being crushed.

It was also important to check whether the swing jaw would fail in either bending or shear.The swing jaw was taken as a simply supported beam with a central load. The maximum bending stress and shear stress were 310 MPa and 103.5 MPa respectively. The ultimate tensile and shear strength of Austenitic Manganese Steel, the swing

jaw material, were 1.65 GPa and 1.17 GPa (Bleck & Haase, 2019). Therefore, the swing jaw had a safety factor of 5 in bending and 9 in shear and thus was safe in operation.

The effect of the rocker on the dynamic crushing torque was as shown in Figure 4.20.

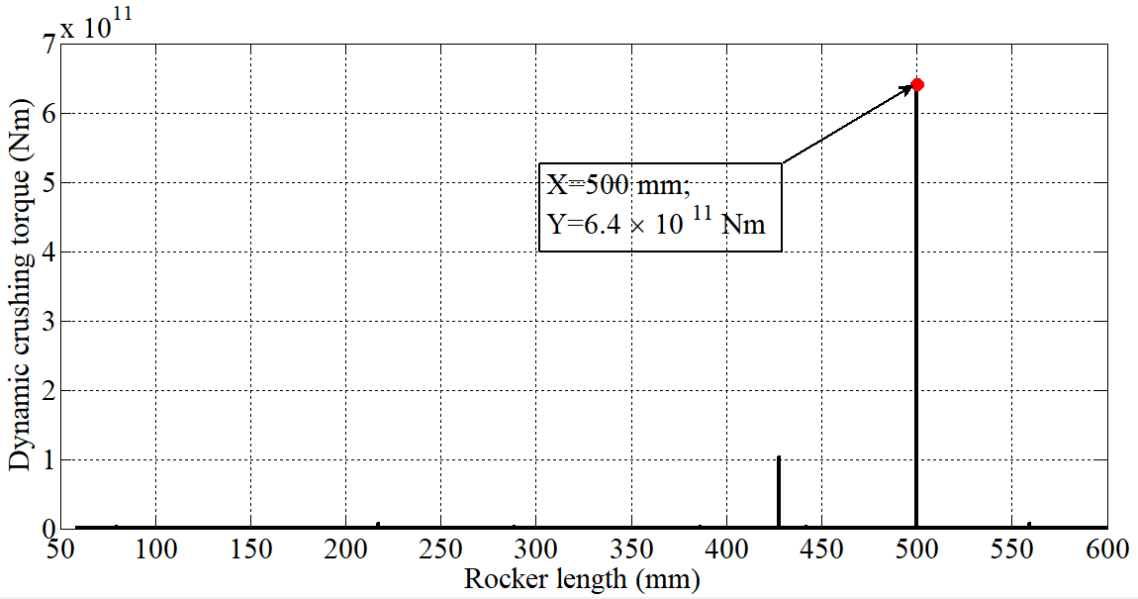

Figure 4.20: Dynamic Crushing Torque vs Rocker Length

The highest peak from the plot was 6.4002×10^{11} Nm at 500 mm. Another prominent peak was observed at 427.5 mm with a magnitude of 1.033×10^{11} Nm. A toggle plate of 500 mm would give the best crushing strength and subsequently the best stone production rate. It would also lead to better energy utilization by proportioning more power to the active crushing stroke than to the idle jaw retraction stroke. At 500 mm rocker length, this design saved 100 mm of link length and thus would lower the cost of fabrication of the jaw crusher.

Finally, the frame length influenced the dynamic torque as shown in Figure 4.21

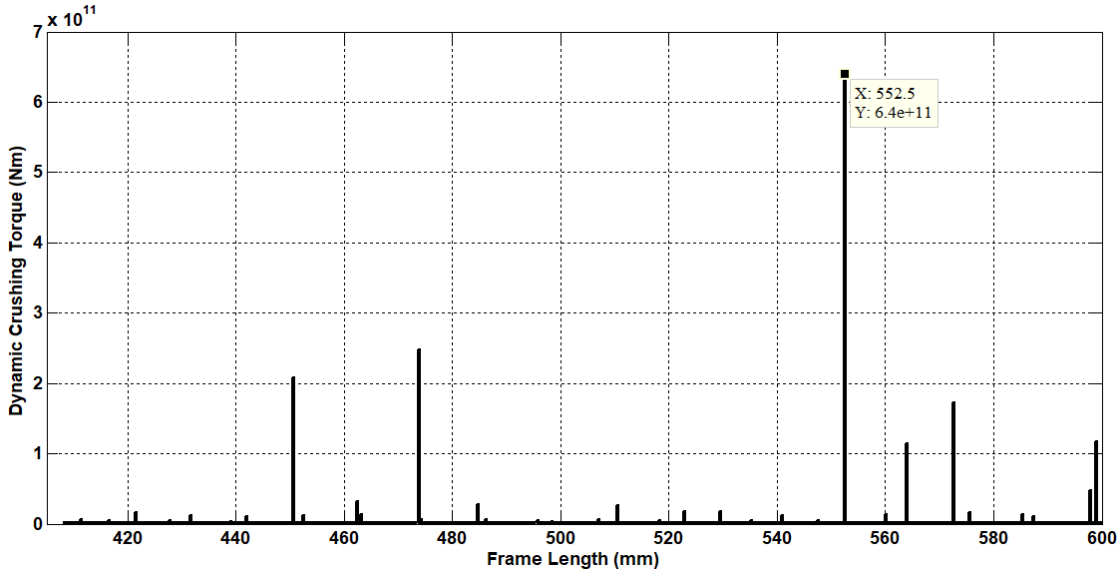

Figure 4.21: Dynamic Crushing Torque vs Frame Length

The greatest torque obtained by varying the frame size was 6.4002×10^{11} Nm at 552.5 mm. This length would give the most efficient crushing and the best stone production rate. Other significant peaks were at 450.6 mm, 473.9 mm, 564 mm, 572.7 mm, and 599 mm whose magnitudes were in the range of $1.15 - 2.48 \times 10^{11}$ Nm. From the several peaks, it can be concluded that the frame provided more options for length choice compared to other links. This, in turn, would give flexibility during installation and maintenance of the jaw crusher. However, the choice of the highest peak at 552.5 mm resulted in a reduction in link material use thus making the final design more cost effective.

From Figure 4.18, 4.19, 4.20 and 4.21, it is evident that the influence of link lengths on the dynamic crushing torque was non-periodic as opposed to monotonic. In previous responses such as the crush travel inverse, there was a consistent trend of decreasing or increasing effect. However, for the dynamic torque, peaks appeared at specific link lengths without any particualr trend. A comparison of the range of torque values for different links was made to determine which link had the most variation as shown in Figure 4.22.

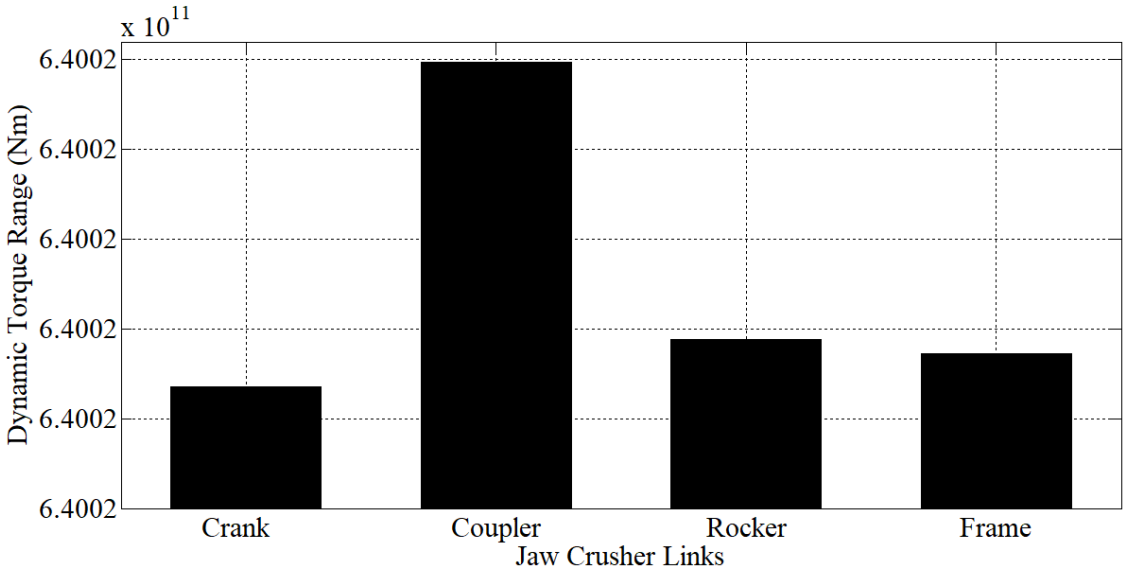

Figure 4.22: Dynamic Torque Range vs Link Type

From Figure 4.22, the coupler had a superior range followed by the rocker, then the frame and finally the crank. The coupler had the highest effect on the dynamic torque hence the biggest variation in torque values. The crank had the least effect amongst the four links.

4.3 Validation

This section validates the single toggle joggle crusher designs obtained using the genetic algorithm (GA) optimisation process. Specifically, this section aims at validating the static torque optimised design by comparing it with another one found in literature by Oduori et al.(M. F. Oduori, Munyasi, & Mutuli, 2016). The parameters to be compared are the crushing stroke and highest torque that can be obtained from the swing jaw for crushing purposes. Table 4.1 shows a comparison of the new optimised design and the one by Oduori et al.(M. F. Oduori et al., 2016).

Table 4.1: Validation of static torque results

Design	Crushing Stroke	Highest Torque(kNm)
Oduori et al.(2016)	181^0	307,857
New Optimised Design	216^0	642,320
Difference (%)	**19.33701657**	**108.6421819**

The optimised static torque design had a longer crushing stroke spanning 36^0 more degrees to register a 19% improvement in crushing. The mechanism is thus capable of crushing more rocks via the increased working stroke. This also makes it a quicker return mechanism than that of Oduori et al.(M. F. Oduori et al., 2016) which reduces the amount of power utilised in the idle retraction stage and dedicating more of the input power to comminution for enhanced stone production.

The two mechanisms were also compared based on the absolute torque values. The highest torque from the optimised design was more than twice that of design by Oduori et al.(M. F. Oduori et al., 2016). Consequently, the new design has greater crushing capability which translates to higher stone production.

There is agreement between the findings of this research and others from other researchers of the single toggle jaw crusher (Luo & Li, 2012; M. F. Oduori et al., 2016; L. Zhang et al., 2012) in some aspects of kinematics. Spefically, the bottom

most point of the jaw crusher experiences the highest difference between shearing and crushing travel. This is true regardless of the profile of both crushing and shearing travels curves which are guided by the link dimensions of a particular crusher.

CHAPTER FIVE

CONCLUSIONS AND RECOMMENDATIONS

5.1 Conclusions

From the outcomes of this research, some conclusions were made. Increasing the length of the toggle plate and reducing the size of the eccentricity helps to improve crushing and reduce shearing problems. Increasing the length of the eccentricity and toggle plate increases the crushing capacity of a jaw crusher. For optimum force transmission, the swing jaw must be longer than the toggle plate, eccentricity and the frame. Unlike other links in the four bar model of the single-toggle jaw crusher, altering the size of the swing jaw has the highest influence on the dynamic crushing torque. The fixed jaw should be inclined as per the inclination of the crushing travel of points on the swing jaw to ensure uniform loading on the jaws and prevent creation of stress concentration points. The fixed jaw should be concave in shape to handle the shearing load from sliding rock materials. A crush travel optimised jaw crusher has the daily capacity to fill a 10 tonne truck when working 8 hours a day.

5.2 Recommendations

This study makes the following recommendations:

1. The optimised designs be fabricated and tested for their crushing performance.
2. Exploration of a single toggle jaw crusher four-bar model where the swing jaw is not the longest link. This could result in higher crushing-to-shear travel ratio.

3. Further study be done to facilitate the design of a support structure for the optimised single-toggle jaw crusher design for vibration reduction.

4. Suitable weighting factors be determined to combine the different optimised designs into one final design via multiobjective optimisation.

REFERENCES

Acharyya, S. K., & Mandal, M. (2009). Performance of EAs for four-bar linkage synthesis. *Mechanism and Machine Theory*, *44*(9), 1784–1794. Retrieved from http://dx.doi.org/10.1016/j.mechmachtheory.2009.03.003 doi: 10.1016/j.mechmachtheory.2009.03.003

Asbjörnsson, G. (2013). Modelling and Simulation of Dynamic Behaviour in Crushing Plants. , 1–53.

Asbjornsson, G. (2015). *Crushing Plant Dynamics* (PhD Thesis, Chalmers University of Technology, Goteborg, Sweden). Retrieved from https://vpp.sbuf.se/Public/Documents/ProjectDocuments/3a758b02-72f0-4b69-b012-87023214661c/FinalReport/SBUF12819SlutredovisningDoktorsavhandlingCrushingPlantDynamics.pdf

Balli, S. S., & Chand, S. (2002). Transmission angle in mechanisms (Triangle in mech). *Mechanism and Machine Theory*, *37*(2), 175–195. doi: 10.1016/S0094-114X(01)00067-2

Bleck, W., & Haase, C. (2019). *Physical metallurgy of high manganese steels* (1st ed., Vol. 9) (No. 10). Basel: MDPI. doi: 10.3390/met9101053

Bloomberg. (2019, jun). *Regional countries plan to go big on infrastructure spending.* Nairobi. Retrieved from https://www.standardmedia.co.ke/business/article/2001329619/eac-states-to-go-big-on-infrastructure-spending

Bozorg-Haddad, O., Solgi, M., & Loaiciga, H. A. (2017). *Meta-Heuristic and Evolutionary Algorithms for Engineering Optimization* (1st ed.). River Street: John Wiley & Sons.

Cao, J., Rong, X., & Yang, S. (2006). Jaw plate kinematical analysis for single

toggle jaw crusher design. *IET Conference Publications*(524), 62–66. doi: 10.1049/cp:20060729

Ceccarelli, M., Ghosh, A., & Corves, B. (2015). *Introduction to Micromechanisms and Microactuators* (1st ed.). New Delhi: Springer. Retrieved from `http://www.springer.com/series/8779`

Doane, J. (2016). *Machine Analysis with Computer Applications for Mechanical Engineers* (1st ed.). Chichester: John Wiley & Sons.

Donovan, J. G. (2003). *Fracture Toughness Based Models for the Prediction of Power Consumption, Production Size and Capacity of Jaw Crushers* (PhD Thesis). Virginia Polytechnic Institute and State University.

Fidanova, S. (2013). *Recent Advances in Computational Optimization.* Cham: Springer International Publishing Switzerland.

Freedonia. (2019). *World Construction Aggregates - Demand and Sales Forecasts, Market Share, Market Size, Market Leaders* (Tech. Rep. No. December). New York: The Freedonia Group, Inc. Retrieved from `https://www.freedoniagroup.com/World-Construction-Aggregates.html`

Garnaik, S. K. (2010). *Computer Aided Design of Jaw crusher* (Bachelor of Technology Thesis, National Institute of Technology Rourkela). Retrieved from `ethesis.nitrkl.ac.in/1812/1/thesis{\_}sobhan.pdf`

Gen, M., & Cheng, R. (2000). *Genetic Algorithms & Engineering Optimization* (1st ed.). Ashikaga: John Wiley & Sons.

Golikov, N., & Timofeev, I. (2018). Determination of capacity of single-toggle jaw crusher, taking into account parameters of kinematics of its working mechanism. *Journal of Physics*, *15*(5).

Gupta, A., & Yan, D. (2006). *Mineral Processing Design and Operation: An Introduction* (1st ed.). Amsterdam: Elsevier B.V.

Gupta, K. C., & Tinubu, S. O. (1983). Synthesis of Bimodal Function Generating Mechanisms Without Branch Defect. *Transaction of the ASME, Journal of Mechanisms, Transmissions and Automation in Design*, *105*(82), 641–647. doi:

10.1115/1.3258528

Huang, P., Lei, Q., & Wang, K. (2011). Simulation Analysis of the Tilted-Jaw Crusher Based on ADAMS. *Advanced Manufacturing Systems*, *201*(2011), 499–503.

Jinxi, C., Zhiyu, Q., Guopeng, W., Xingfu, R., & Shichun, Y. (2007). Investigation on Kinetic Features of Multi-Liners in Coupler Plane of Single Toggle Jaw Crusher. *IEEE*(2), 1639–1642.

Jinxi, C., Zhiyu, Q., Xingfu, R., & Shichun, Y. (2007). Experimental Research on Crushing Force and its Distribution Feature in Jaw Crusher. In *Second ieee conference on industrial electronics and applications* (pp. 2143–2147). Taiyuan, China: IEEE Xplore.

Kinzel, E. C., Schmiedeler, J. P., & Pennock, G. R. (2006). Kinematic Synthesis for Finitely Separated Positions Using Geometric Constraint Programming. *Journal of Mechanical Design*, *128*(5), 1070. Retrieved from `http://mechanicaldesign.asmedigitalcollection.asme.org/article.aspx?articleid=1449103` doi: 10.1115/1.2216735

Kirankumar, G. (2014). Optimization of Jaw Crusher. *Advance Research and Innovations in Mechanical, Material Science, Inudstrial Engineering and Management*, 238–242.

Kiusalaas, J. (2009). *Numerical Methods in Engineering with MATLAB ®*. Retrieved from `http://www.amazon.com/Numerical-Methods-Engineering-MATLAB-Kiusalaas/dp/0521191335` doi: 10.1017/CBO9780511812200

Kramer, O. (2017). *Genetic Algorithm Essentials* (1st ed.). Oldenburg: Springer International Publishing AG.

Krishnamurty, S. (1989). *Multiple Objective Optimization Techniques in the Synthesis and Design of Mechanisms* (1st ed.). Madison: University of Wisconsin.

Kunjur, A., & Krishnamurty, S. (1997). Genetic Algorithms in Mechanical Synthesis. *Journal of Applied Mechanisms and Robotics*, *4*(2), 18–24.

Kureichik, V. M., Malioukov, S. P., Kureichik, V. V., Malioukov, A. S., Dempsey, V. I., & Neill, M. O. (2009). *Genetic Algorithms for Applied CAD Problems* (1st ed.). Berlin: Springer-Verlag Berlin Heidelberg.

La-la, Z., Zhong-bin, W., & Feng, Z. (2008). Multi-object optimization design for differential and grading toothed roll crusher using a genetic algorithm. *Journal of China University of Mining and Technology*, *18*(September 2007), 316–320.

Langat, A. (2019, sep). *Chinese Contractor Adopts Manufactured Sand in Quest for Alternative to Natural Sand.* Nairobi. Retrieved from `https://chinaafricaproject.com/analysis/kenya-china-sand-sustainability-construction-anthony-langat/`

Laribi, M. A., Mlika, A., Romdhane, L., & Zeghloul, S. (2004). A combined genetic algorithm-fuzzy logic method (GA-FL) in mechanisms synthesis. *Mechanism and Machine Theory*, *39*(7), 717–735. doi: 10.1016/j.mechmachtheory.2004.02.004

Lee, E. (2012). *Optimization of Compressive Crushing* (PhD Thesis, Chalmers University of Technology). Retrieved from `http://publications.lib.chalmers.se/records/fulltext/157884.pdf`

Li, X., & Wang, G. (2006). Optimum design of compound pendulum jaw crusher with genetic algorithms. *Construction Machinery*, *1*(6), 55–62.

Lin, C. C., & Chang, W. T. (2002). The force transmissivity index of planar linkage mechanisms. *Mechanism and Machine Theory*, *37*(12), 1465–1485. doi: 10.1016/S0094-114X(02)00070-8

Lin, W. Y. (2010). A GA-DE hybrid evolutionary algorithm for path synthesis of four-bar linkage. *Mechanism and Machine Theory*, *45*(8), 1096–1107. Retrieved from `http://dx.doi.org/10.1016/j.mechmachtheory.2010.03.011` doi: 10.1016/j.mechmachtheory.2010.03.011

Lindqvist, M., & Evertsson, C. M. (2003). Linear wear in jaw crushers. *Minerals Engineering*, *16*(1), 1–12. doi: 10.1016/S0892-6875(02)00179-6

Liu, X.-J., & Wang, J. (2014). *Parallel Kinematics* (1st ed.). Heidelberg: Springer

Science & Business Media. doi: 10.1007/978-3-642-36929-2

Luo, Z., & Li, S. (2012). Optimization Design for Crushing Mechanism of Double Toggle Jaw Crusher. *Applied Mechanics and Materials*, *202*(1), 312–316. doi: 10.4028/www.scientific.net/AMM.201-202.312

Mandl, G. (1999). *Faulting in Brittle Rocks: An Introduction to the Mechanics of Tectonic Faults*. Graz: Springer Science & Business Media.

Mcdougall, R., & Nokleby, S. (2008). Synthesis of Grashof four-bar mechanisms using Particle Swarm Optimization. In *Proceedings of the asme 2008 international design engineering technical conferences & computers and information in engineering conference* (pp. 1–5). Brooklyn: IDETC/CIE 2008.

McNally, G. (2003). *Soil and Rock Construction Materials* (3rd ed.). London: E & FN SPON.

Michalewicz, Z. (1996). *Genetic Algorithms + Data Structures = Evolution Programs* (3rd ed.). Charlotte: Springer Science & Business Media. doi: 10.1007/978-3-662-03315-9

Miller, R. (2009). Designing a new crushing technique to combine impact and compression fracturing in a rock crushing chamber. *Proceedings of the International Center for Aggregate Research Symposium, ICAR,USA*.

Mu, F., Lio, C., Li, H., Deng, L., & Huang, S. (2013). Application of Signal Feature Extraction of Double Cavity Jaw Crusher Based on DEPSO. *Journal of Computers*, *8*(2), 448–454. Retrieved from `https://pdfs.semanticscholar.org/5c17/97c40f17aa9d4378f83eaff9dca3d590312a.pdf` doi: 10.4304/jcp.8.2.448-454

Mugambi, A. (2017). *Optimism as Researchers Present Midterm Progress Reports.* Retrieved 2020-06-22, from `http://jkuat.ac.ke/projects/africa-ai-japan/optimism-researchers`

Muiruri, P. (2019, feb). *SGR sand made from rocks.* Nairobi. Retrieved from `https://www.standardmedia.co.ke/business/article/2001314784/bad-news-if-you-want-to-sell-sand-for-sgr-phase-two`

Munyasi, M., & Oduori, M. F. (2012). *An Overview of the Small Scale Stone Crushing Industry in Western Kenya* (Tech. Rep.). Nairobi: UoN.

Mwafrika. (2018). *Stone Crushers In Kenya.* Retrieved 2019-12-28, from `http://mwafrikaballastcrushers.com/home/20-8t-premium-advance.html`

Myszka, D. H. (2012). *Machines and Mechanisms* (4th ed.). New Jersey: Prentice Hall.

Nedic, N., Prsic, D., Dubonjic, L., Stojanovic, V., & Djordjevic, V. (2014). Optimal cascade hydraulic control for a parallel robot platform by PSO. *International Journal of Advanced Manufacturing Technology*, *72*(5), 1085–1098. Retrieved from `https://doi.org/10.1007/s00170-014-5735-5` doi: 10.1007/s00170-014-5735-5

Oduori, M., Mutuli, S., & Munyasi, D. (2015). Analysis of the single toggle jaw crusher kinematics. *Journal of Engineering, Design and Technology*, *13*(2), 231–239. doi: 10.1108/JEDT-01-2013-0001

Oduori, M. F., Munyasi, D. M., & Mutuli, S. M. (2016). Analysis of the single toggle jaw crusher force transmission characteristics. *Journal of Engineering (United Kingdom)*, *2016*(November), 28–36. Retrieved from `https://doi.org/10.1155/2016/1578342` doi: 10.1155/2016/1578342

Panigrahi, B. K., Abraham, A., & Das, S. (2010). *Computational Intelligence in Power Engineering* (1st ed.). Chennai, Inida: Springer-Verlag Berlin Heidelberg.

Patel, S. R., Patel, D. S., & Patel, B. D. (2013). A Review on Kinematic and Dynamic Analysis of Mechanism. , *2*(2), 338–341.

Paterson, M. S., & Wong, T. (2005). Experimental Studies on the Brittle Fracture Stress. *Experimental Rock Deformation - The Brittle Field*, 17 – 44. doi: 10.1007/3-540-26339-X_3

Persson, P.-A., Holmberg, R., & Lee, J. (2000). *Rock Blasting and Explosives Engineering.* Socorro: CRC Press.

Podra, P., & Andersson, S. (1999). Simulating sliding wear with finite element

method. *Tribology International*, *32*(2), 71–81.

Raju Bahubalendruni, D. (2017). Numerical Analysis for Force Distribution along the Swing Jaw Plate of a Single Toggle Jaw Crusher. *World Journal of Engineering*, *14*(3).

Rattan, S. (2009). *Theory of Machines* (4th ed.). New Delhi: Tata McGraw Hill Education Private Limited.

Roston, G. P., & Sturges, R. H. (1996). Genetic algorithm synthesis of four-bar mechanisms. *Artificial Intelligence for Engineering, Design, Analysis and Manufacturing*, *10*(05), 371–407. doi: 10.1017/S0890060400001700

Rumbarger, J. (2003). *Architectural Graphic Standards for Residential Construction: The Architect's and Builder's Guide to Design, Planning, and Construction Details* (1st ed.). Hoboken, USA: John Wiley & Sons.

Rusiński, E., Moczko, P., Pietrusiak, D., & Przybyłek, G. (2013). Experimental and numerical studies of jaw crusher supporting structure fatigue failure. *Strojniski Vestnik/Journal of Mechanical Engineering*, *59*(9), 556–563. doi: 10.5545/sv-jme.2012.940

SCM. (2020). *PE Jaw Crusher.* Retrieved 2021-02-15, from `https://johnspizza.pl/products/pe-jaw-crusher.html`

Shinde, A. S., Kulkarni, S. A., & Shete, S. S. (2017). Dimensional Synthesis of Four Bar Mechanism Using Genetic Algorithm. *International Journal of Current Engineering and Technology*, *7*(4), 1572–1580.

Shrivastava, A. K., & Sharma, A. (2012). A review on study of jaw crusher. , *2*(3), 885–888.

Siekmann, J., & Wahlster, W. (2013). *Intelligent Robotics and Applications* (Vol. 8102). Retrieved from `http://link.springer.com/10.1007/978-3-642-40852-6` doi: 10.1007/978-3-642-40852-6

Sivanandam, S., & Deepa, S. (2008). *Introduction to Genetic Algorithms* (1st ed.). Heidelberg Printed: Springer Science & Business Media. Retrieved from `https://doi.org/10.1007/s00170-014-5735-5`

Stanisic, M. (2015). *Mechanisms and Machines: Kinematics, Dynamics, and Synthesis* (1st ed.). Stamford: Cengage Learning.

Starosta, R. (2008). Application of Genetic Algorithm and Fourier Coefficients (Ga-Fc) in Mechanism Synthesis. *Theoretical And Applied Mechanics*, *46*(2), 395–411.

Suresh, B. A. (2009). *Computer Aided Design and Analysis of Swing Jaw Plate of Jaw Crusher* (Master of Technology). National Institute of Technology,Rourkela.

Svedensten, P., & Evertsson, C. M. (2005). Crushing plant optimisation by means of a genetic evolutionary algorithm. *Minerals Engineering*, *18*(5), 473–479. doi: 10.1016/j.mineng.2004.08.008

Sverdrup, H. U., Koca, D., & Schlyter, P. (2017). A Simple System Dynamics Model for the Global Production Rate of Sand, Gravel, Crushed Rock and Stone, Market Prices and Long-Term Supply Embedded into the WORLD6 Model. *BioPhysical Economics and Resource Quality*, *2*(2), 1–20. Retrieved from `https://link.springer.com/content/pdf/10.1007/s41247-017-0023-2.pdf` doi: 10.1007/s41247-017-0023-2

Terva, J., Kuokkala, V.-T., Valtonen, K., & Siitonen, P. (2017). Effects of compression and sliding on the wear and energy consumption in mineral crushing. *Wear*, *12*(4). Retrieved from `https://doi.org/10.1016/j.wear.2017.12.004` doi: 10.1016/j.wear.2017.12.004

Tests, F. (2015). PPT Fatigue tests and stress-life. *Internet*.

Thuita, P. (2017, aug). *Tough times ahead for builders as Kenya runs out of gravel.* Nairobi. Retrieved from `https://www.constructionkenya.com/4639/kenya-gravel-shortage/`

Tong, Y., Myszka, D. H., & Murray, A. P. (2013). *Four-Bar Linkage Synthesis for a Combination of Motion and Path-Point Generation* (Masters Thesis, University of Dayton). doi: 10.1115/DETC2013-12969

Unland, G., & Szczelina, P. (2004). Coarse crushing of brittle rocks by compression.

International Journal of Mineral Processing, *74*(SUPPL.), 209–217. doi: 10 .1016/j.minpro.2004.07.030

Venkataraman, P. (2002). *Applied Optimization with MATLAB Programming* (1st ed.). New York: John Wiley & Sons.

Wairimu, W. (2015). *Micro, Small and Medium-Size Enterprises (MSMEs) as Suppliers to the Extractive Industry* (Tech. Rep. No. January). Nairobi: UNDP.

Waldron, K., Kinzel, G., & Agrawal, S. (2016). *Kinematics, Dynamics, and Design of Machinery*. Chichester: John Wiley & Sons.

Wang, J., Qin, B., Zhang, W., & Yang, B. (2012). Hydraulic support four-bar linkage optimized design based on particle swarm optimization. *Proceedings of the 2012 International Conference on Industrial Control and Electronics Engineering, ICICEE 2012*, *3*(12), 291–294. doi: 10.1109/ICICEE.2012.84

Wills, B. A., & Napier-Munn, T. (2006). *Mineral Processing Technology* (7th ed.). Brisbane, Australia: Elsevier Science & Technology Books.

Wilson, B. (2007). *Igneous Petrogenesis A Global Tectonic Approach* (1st ed.). Dordrecht: Springer Science & Business Media.

Yang, X.-S. (2010). *Engineering Optimization: An Introduction with Metaheuristic Applications* (1st ed.). Hoboken: John Wiley & Sons.

Yao, M., & Page, N. W. (2000). Influence of comminution products on abrasive wear during high pressure crushing. *Wear*, *242*(1-2), 105–113. doi: 10.1016/ S0043-1648(00)00410-5

Zhang, L., Shen, X., Cao, S., & Lv, C. (2012). Application of Orthogonal Experiments in Simulation and Optimization of Jaw Crusher on Traveling Characteristic Value of Moving Jaw. *Applied Mechanics and Materials*, *216*(10), 101–104. doi: 10.4028/www.scientific.net/AMM.215-216.101

Zhang, X. B., & Li, J. (2008). A failure criterion for brittle and quasi-brittle materials under any level of stress concentration. *Engineering Fracture Mechanics*, *75*(17), 4925–4932. Retrieved from `http://dx.doi.org/10.1016/`

j.engfracmech.2008.06.020 doi: 10.1016/j.engfracmech.2008.06.020

Zhangfeng, Z., Yanbiao, L., Wenhao, L., Xian, Z., Xingliang, Z., & Jiang, Z. (2015). Research on the biaxial compound pendulum jaw crusher based on seven-bar mechanism. *Journal of Mechanical Engineering Science*, *0*(0), 1–14. doi: 10.1177/0954406215583889

Zhou, H., & Cheung H.M., E. (2001). Optimal synthesis of crank-rocker linkages for path generation using the orientation structural error of the fixed link. *Mechanism and Machine Theory*, *36*(8), 973–982. doi: 10.1016/S0094-114X(01)00029-5

Appendices

APPENDIX A

I: Motion Optimisation Code

```
%% Objective Function definition
function y = Optimisation_with_GA(x)

%% parameters
L_1=x(1);% eccentricity/ crank length (a)
L_2=x(2);% swing jaw/ coupler length (b)
L_3=x(3);% toggle plate/ rocker length (c)
L_0=x(4); %frame length (d)

%% Time and speed definitions
t=0:pi/(18*360):pi/18; % definition of time steps for one complete
revolution
ang_speed=36;% speed of driving shaft
thetA=ang_speed*t;

%% Position Analysis for each instance of time

for i=1:length(t)
i;
theta=thetA(i);
P1=[0;0];
P4=L_0*[1;0];
```

```
P2=L_1*[cos(theta); sin(theta)];
P2_counter(:,i)=P2;
E=sqrt(L_1^2 + L_0^2 -2*L_1*L_0*cos(theta));
alfa=asin(L_1*sin(theta)./E);
beta = acos((E.^2+ L_3^2-L_2^2)./(2*E*L_3));
P3=[L_0-L_3*cos(alfa+beta);L_3*sin(alfa+beta)];
P3_counter(:,i)=P3;
slope= (P3(2,:)-P2(2,:))./(P3(1,:)-P2(1,:));
L3_points=linspace(0,L_2,361); % Discretisation of swing jaw into

P_X=P2(1,:)+L3_points*cos(atan(slope));
P_XX(:,i)=P_X;
P_Y=P2(2,:)+L3_points*sin(atan(slope));
P_YY(:,i)=P_Y;
i=i+1;
end

%% minimum value for each point on BC
min_TR_X=min(P_XX,[],2);
max_TR_X=max(P_XX,[],2);
min_TR_Y=min(P_YY,[],2);
max_TR_Y=max(P_YY,[],2);

%% Ranges of travel in crushing (Y-DIRECTION) and Shearing
(X-DIRECTION)

TRAVEL_RANGE_X=max_TR_X-min_TR_X;
TRAVEL_RANGE_Y=max_TR_Y-min_TR_Y;
```

```
%% AREA UNDER CURVE
A_X= trapz(L3_points,TRAVEL_RANGE_X);
A_Y= trapz(L3_points,TRAVEL_RANGE_Y);

%% OBJECTIVE FUNCTIONS
%% NB:Choose one of the two:
% For shearing-to-crushing-ratio choose the FIRST
% For Crush travel inverse choose the SECOND


y= A_X/A_Y; %shearing-crushing ratio
% y=1/A_Y; % crush travel inverse ratio

end
```

APPENDIX B

II: Static Crushing Force Optimisation Code

```
function y = static_objective_func(x)
% % parameters
a=x(1);% eccentricity/ crank length (a)
b=x(2);% swing jaw/ coupler length (b)
c=x(3);% toggle plate/ rocker length (c)
d=x(4); %frame length (d)

%% Initialising crank angle theta
theta(1)=0;

%% Iterations for all time intervals
for i=1:360;
%% solving for constants in output angle (phi) equation
k= ((a^2-b^2+c^2+d^2))/2;
A=k-a*(d-c).*cosd(theta)-c*d;
B=-2*a*c.*sind(theta);
C=k-a*(d+c).*cosd(theta)+c*d;
%% definition of mechanism angles
phi=2*atand((-B-sqrt((B.^2)-(4*A.*C))./(2*A));%valid case
V=(((c*sind(phi))-(a*sind(theta)))/b);
```

```
beta=asind(((c.*sind(phi))-(a.*sind(theta)))./b);


%% Crusher Forces based on strengh of granite rock
% crushing force
P_C=(13.8)*b^2;%N
% shear force
P_S=1.86*b^2;%N

%% External force due to weight of stones
volume=0.5*((19.5+270)*b*(cosd(beta))*(b/10));% volume of crushing
chamber
density=2750e-9; %kg/mm^3 % density of granite
packing_factor=0.6; % stone packing factor
F=packing_factor*volume*density*9.81; % weight of stones


%%  input torque
T2=(2500/3)*1e3; %Nmm
%% Joint force f_43

f_43=(T2-((a.*P_C*cosd(theta-beta))+(a*P_S*sind(theta-beta))+(a*F*sind(theta))))
/(a.*sind(theta-phi))  ;

%% Output torque at the swing jaw
T3=-(b/2)*(F.*sind(beta)+P_C +2*f_43.*sind(beta-phi));
T_3C(i)=T3/T2; %storing torque values for every theta instance
theta=theta+1;
i=i+1;
```

```
end

%% Integrating all crushing torques
T_3CC=T_3C(T_3C>0); %array of positive torques
n=length(T_3CC); % number of elements in array
T=(trapz(T_3CC))/n; %total static crushing torque
y=1/T; %objective function involving inverse of torque
end
```

APPENDIX C

III: Dynamic Crushing Force Optimisation Code

```
function y = force_objective_fxn(x)

%% parameters
a=x(1);% eccentricity/ crank length (a)
b=x(2);% swing jaw/ coupler length (b)
c=x(3);% toggle plate/ rocker length (c)
d=x(4); %frame length (d)

%% masses
%% crank
rho= 7900; %kg/m^3 (Low Alloy Steel)
Area_2=(a/10)^2;
vol_2=Area_2*a;
m_2=rho*vol_2;

%% coupler
Area_3=(b/10)^2;
vol_3=Area_3*b;
m_3=rho*vol_3;
%% rocker
```

```
Area_4=(c/10)^2;
vol_4=Area_4*c;
m_4=rho*vol_4;

%% Initialising a 9 X 9 matrix to store the 9 equilibrium\\ equations
for the three links( crank, coupler, rocker) for 360 steps
soln=ones(9,361);
theta(1)=1;
theta_array=ones(1,361);


%% for loop to achieve 360 steps
for i=1:360
%% constants required to solve output angle (phi)
k= ((a^2-b^2+c^2+d^2))/2;
A=k-(a*(d-c)*cosd(theta))-c*d;
B=-2*a*c*sind(theta);
C=k-(a*(d+c)*cosd(theta))+(c*d);
phi=2*atand((-B-sqrt((B.^2)-(4*A.*C)))./(2*A));%rocker angle
beta=acosd((d+c*cosd(phi)-a*cosd(theta))/b); %coupler angle
bet_ray(i)=beta;
%% Defining angular velocities
omega_2=36 ;%\omega_2 in rad/s
omega_4= (a*omega_2*sind(beta-theta))/(c*sind(beta-phi));
omega_3= -(a*omega_2*sind(phi-theta))/(b*sind(phi-beta));
%% angular accelerations
alpha_2=0; %rad/s^2
alpha_b=((a*alpha_2*sind(phi-theta)-(a*omega_2^2)*(cosd(phi-theta))-((b*omega_3^2
alpha_c=((a*alpha_2*sind(beta-theta)-(a*omega_2^2)*(cosd(beta-theta))-(b*omega_3^
```

```
%% X matrix to store the variables on the LHS of the 9 equilibrium
equations
A_71=-(a/2)*sind(theta) ;
A_72=(a/2)*cosd(theta) ;
A_73=-(a/2)*sind(theta) ;
A_74=(a/2)*cosd(theta);

A_83=-(b/2)*sind(beta) ;
A_84=(b/2)*cosd(beta);
A_85=-(b/2)*sind(beta) ;
A_86=(b/2)*cosd(beta);



A_95=(c/2)*sind(phi) ;
A_96=-(c/2)*cosd(phi) ;
A_97=-(c/2)*sind(phi) ;
A_98=(c/2)*cosd(phi);

X=[1 0 -1 0 0 0 0 0 0 ;0 1 0 -1 0 0 0 0 0 ; 0 0 1 0 -1 0 0 0 0 ;0 0 0
1 0 -1 0 0 0 ;0 0 0 0 1 0 1 0 0 ;0 0 0 0 0 1 0 1 0 ; A_71 A_72 A_73
A_74 0 0 0 0 0;0 0 A_83 A_84 A_85 A_86 0 0 1;0 0 0 0 A_95 A_96 A_97
A_98 0];

X(isnan(X))=0.1;% To avoid trivial and singular matrices

%% Defining compressive force required to break rocks
P_C=(138e5)*b^2;%N
P_S=(18.6e4)*b^2;%N
%% External force due to weight of stones
```

```
volume=0.5*((19.5+270)*1e-3)*b*(cosd(beta))*(b/10);
density=2750; %kg/m^3
packing_factor=0.6;
F=packing_factor*volume*density*9.81;
%% Defining acceleration of link centres
%% ACCELERATION OF THE CENTER OF MASS OF LINK 2
omega_2 =[0 0 omega_2];
r_G2A=(a/2)*[cosd(theta) sind(theta) 0];
V_G2=cross(omega_2,r_G2A);
a_G2=cross(omega_2,V_G2);
aG2_x=a_G2(1);
aG2_y=a_G2(2);
%% ACCELERATION OF THE CENTER OF MASS OF LINK 3
%FoRMULA: aG3=a_B+a_G3/B=a_B+omega_3 X (omega_3 X r_G3B)+( alpha_3 X
X r_G3B)
%first calculate position vector of point B
r_B= a*[cosd(theta) sind(theta) 0];

% then calculate the velocity vector  of the same point B using the
cross product omega_2 CROSS r_B
V_B = cross(omega_2,r_B);
%then calculate the acceleration of point B using the CROSS PRODUCT
of omega_2 and V_B
a_B=cross(omega_2, V_B);
% Now to the second component of the formula......omega_3 X (omega_3
X r_G3B)+( alpha_3 X X r_G3B).......
% this has two part, the normal acceleration....omega_3 X (omega_3 X
r_G3B)
%  and the tangential acceleration.......( alpha_3 X X r_G3B)
```

```
% then add the two
%starting with the normal acceleration part
%This requires the calculation of the postion vector r_G3B
r_G3B=(b/2)*[cosd(beta) sind(beta) 0];
% And define omega_3 as a vector
omega_3=[0 0 omega_3];
a_G3B_n= cross(omega_3,cross(omega_3,r_G3B));
% then the second part of tangential acceleration
%But forst define alpha_3 as a vector
alpha_3=[0 0 alpha_b];
a_G3B_t=cross(alpha_3,r_G3B);
% summing the two parts
a_G3=a_B+a_G3B_n+a_G3B_t;
% then subdivide the vector into the x and y components
aG3_x=a_G3(1); % x coordinate
aG3_y=a_G3(2);  % y coordinate
%% ACCELERATION OF THE CENTER OF MASS OF LINK 4
%FoRMULA: aG4=omega_4 X (omega_4 X r_G4D)+( alpha_4 X r_G3D)
% AGAIN, this has two parts,...
% the normal acceleration part.....omega_4 X (omega_4 X r_G4D)   AND
%the tangential acceleration part.....( alpha_4 X r_G3D)
%Now for part One(NORMAL)...
%first calculate position vector of point G3 wrt to D
r_G4D=(c/2)*[cosd(phi) sind(phi) 0];
%Then the normal acceleration becomes
%But first define omega_4 as a vector
omega_4=[0 0 omega_4];
a_G4D_n=cross(omega_4,cross(omega_4,r_G4D));
% The second part(TANGENTIAL)...
```

```
%But forst define alpha_4 as a vector
alpha_4=[0 0 alpha_c];
a_G4D_t=cross(alpha_4,r_G4D);
% Therefore, the total acceleration of point G4 is...
a_G4=a_G4D_n+a_G4D_t;
% AND the x and y components
aG4_x=a_G4(1);
aG4_y=a_G4(2);
%% defining gravity
g=9.81;
%% Input torque
T_2=(2500)/3; %Nm

%% Moments of Inertia for the links

I_zz_2=(m_2*1.01*b^2)/12;%kgm^2
I_zz_3=(m_3*1.01*c^2)/12;%kgm^2
I_zz_4=(m_4*1.01*d^2)/12;%kgm^2



%% Defining column vector Y to store values on the RHS of the
equilibrium equations

Y=[m_2*aG2_x-m_2*g;m_2*aG2_y;m_3*aG3_x-m_3*g-F-P_C*sind(beta)-P_S*cosd(beta);m_3*

%% Solving the dynamic problem
soln=X\Y; % solution of the 8 forces and input torque
solns(:,i)=soln; %matrix of solutions
theta_array(1,i)=theta;% array of theta
```

```
theta=theta+1; %theta incrementals
i=i+1;% incrementals of crank angle instances

end
%% Passing solutions to the respective variables
R12_X=solns(1,:);
R12_Y=solns(2,:);
R32_X=solns(3,:);
R32_Y=solns(4,:);
R43_X=solns(5,:);
R43_Y=solns(6,:);
R14_X=solns(7,:);
R14_Y=solns(8,:);
T_3=solns(9,:);


%% Integrating all dynamic crushing torques
T_3CC=T_3C(T_3C>0); %array of positive dynamic torques
n=length(T_3CC); % number of elements in array
T=(trapz(T_3CC))/n; %total dynamic crushing torque
y=1/T; %objective function involving inverse of dynamic torque

end
```

APPENDIX D

IV:Genetic Algorithm Constraint Function Code

```
function [c,c_eq] =nonlcon(x)
%% Grashofs constraint
c(1)=x(1)+x(2)-x(3)-x(4);
%% Coupler x(2) is longest while crank x(1) is shortest
c(2)=x(1)-x(2);  % crank shorter than coupler
c(3)=x(1)-x(3);   % crank shorter than rocker
c(4)=x(1)-x(4);  % crank shorter than frame
c(5)=-x(2)+x(3);  % coupler longer than rocker
c(6)=-x(2)+x(4);   % coupler longer than frame
%% Ensuring transmission angle is between 40 and 140 degrees
c(7)= -2*x(2)*x(3)*cosd(40)+x(2)^2+x(3)^2-(x(4)-x(1))^2; %minimum
transmission angle
c(8)=-x(2)^2-x(3)^2-2*x(2)*x(3)*cosd(140)-(x(1)+x(4))^2; %maximum
transmission angle
%% equality constraint matrix compulsory but blank
c_eq=[];
end
```